Experimental and Theoretical Studies on the Dynamics of the O(^{3}P) + Propene Reaction: Primary Products, Branching Ratios, and Role of Intersystem Crossing

Francesca Leonori, Nadia Balucani, Vaclav Nevrly,[†] Astrid Bergeat,[‡] Stefano Falcinelli,[§] Gianmarco Vanuzzo, and Piergiorgio Casavecchia*

Dipartimento di Chimica, Biologia e Biotecnologie, Università degli Studi di Perugia, 06123 Perugia, Italy

Carlo Cavallotti*

Dipartimento di Chimica, Materiali e Ingegneria Chimica "Giulio Natta", Politecnico di Milano, 20131 Milano, Italy

1. INTRODUCTION

Small unsaturated hydrocarbons are crucial intermediates in the combustion of most fuels[1,2] and are involved in the generation of polycyclic aromatic hydrocarbons and soot. The prevalent consumption pathways of small unsaturated hydrocarbons in combustion systems are their reactions with ground-state ^{3}P oxygen atoms. A complete understanding of combustion processes, especially as far as the formation of pollutants is concerned, requires the knowledge at the molecular level of all the important elementary reactions. Since the products of one elementary reaction become the reactants of a subsequent one in propagating or terminating chains, it is very important to determine the identity of the primary reaction products and their branching ratios (BRs). Only in this way we might be able to understand and, possibly, control the formation of combustion pollutants.[1,2] Rate coefficients for most combustion reactions have been measured in kinetics experiments,[3] but much less is known about the nature of the primary products and their BRs. In spite of their apparent simplicity, the elementary reactions of O(^{3}P) with unsaturated hydrocarbons are actually multichannel reactions involving important non-adiabatic effects, and the product identities as well as their relative yields have not been easy to determine, especially under the conditions (particularly temperature) that resemble those of flames.

The determination of the reaction products and their yields remains difficult to achieve in kinetics experiments, and a complementary method, the crossed-molecular-beam (CMB) technique in its "universal" arrangement with mass spectrometric (MS) detection, represents an efficient experimental alternative to investigate polyatomic multichannel elementary reactions and provide useful additional information. In

particular, CMB experiments with MS detection and time-of-flight (TOF) analysis, based on "soft" ionization by low energy electrons[4] or tunable vacuum ultraviolet (VUV) synchrotron radiation,[5] have proved to be particularly suitable to unambiguously identify the primary reaction products of multichannel reactions. The implementation of the "soft" ionization technique has been crucial because it can mitigate or suppress dissociative ionization of products and/or interfering species, which has been the main limitation in typical CMB-MS experiments based on "hard" ionization (with electron energy of 60−200 eV). In any case MS detection is advantageous for systems like these, where complex polyatomic radicals are produced and spectroscopic techniques cannot be in general applied, because it permits us to interrogate all channels on the same footing.

In our laboratory we have undertaken a systematic experimental investigation of $O(^3P)$ reaction dynamics with unsaturated hydrocarbons. For $O(^3P) + C_2H_2$ and $O(^3P) + C_2H_4$, by exploiting soft electron−ionization (EI) detection we have identified and characterized the dynamics of essentially all the open channels at collision energies, E_c, corresponding to high temperatures.[6−8] For the reaction $O(^3P) + C_2H_4$, we have observed some primary reaction products that can only be formed after intersystem crossing (ISC) to the singlet potential energy surface (PES) takes place.[7,8] We remind that in $O(^3P)$ reactions with closed-shell molecules the reactants approach on a triplet PES which always intersects a singlet PES usually supporting a stable intermediate. ISC is then possible from the triplet to the singlet PES, making the dynamics which involve motion on the underlying singlet PES different from those involving motion only over the triplet PES. Previous measurements of the reactive scattering of $O(^3P)$ with various alkyl iodides have indicated the occurrence of ISC.[9−11] Nevertheless, the investigation of atomic oxygen reactions with small molecules containing light atoms, such as $O + H_2S$, clearly excluded the occurrence of ISC,[12] leading to the conclusion that ISC could be significant only in the presence of heavy atoms because of the larger spin−orbit coupling. In this respect, it came as a surprise that for the reaction $O(^3P) + C_2H_4$ ISC accounts for about 50% of the total reactivity[7,8] and even more for the reactions $O(^3P) + CH_2CCH_2$[13] and $O(^3P) + CH_3CCH$.[14] The role of ISC in the $O(^3P) + C_2H_4$ reaction has been confirmed by detailed theoretical work.[7,8,15] The central role of ISC in this family of reactions, specifically in the reactions O + ethylene and O + allene, was established experimentally by the pioneering CMB studies by Lee and co-workers in the late 1980s−early 1990s.[16,17]

It should be noted that, although so far the role of ISC in $O(^3P)$ reactions with unsaturated hydrocarbons has been observed experimentally to increase with increasing molecular complexity (from negligible in $O + C_2H_2$[6] to about 50% in $O + C_2H_4$[7,8] and about 90% in $O(^3P) + C_3H_4$ (allene)[13]), the extent of ISC is in general unpredictable. On one side one may think that the more stable the initial triplet diradical addition intermediate is, the higher the probability of ISC to the singlet PES becomes. However, this argument does not take into account the relative probability of evolution of the triplet intermediate to other outcome channels, which depends on relative barrier heights for isomerization and dissociation and on the location of seams of triplet−singlet PES intersections. Therefore, accurate theoretical treatments for these systems necessarily require the inclusion of nonadiabatic effects. The treatment of nonadiabatic effects in the dynamics of polyatomic

reactive systems remains a challenging task; however, high-level electronic structure calculations of triplet and singlet PESs, including nonadiabatic coupling terms, have become available, and quasiclassical trajectory (QCT) surface-hopping calculations have been used successfully for treating the dynamics of $O + C_2H_4$ employing full-dimensional *ab initio* coupled triplet and singlet PESs[7,8] and of $O + C_2H_4$[15] and $O + C_2H_2$[18] employing direct (on-the-fly) methods. Statistical Rice−Ramsperger−Kassel−Marcus/Master Equation (RRKM/ME) calculations of product BRs have been also performed on those two systems, but they were confined to adiabatic triplet and singlet PESs.[19,20] These recent experimental and theoretical studies on the simpler systems have shown that the extent of ISC in $O(^3P)$ atom reactions with unsaturated hydrocarbons and its effect on the product yields are one of the central issues in this class of combustion reactions.

Because of the difficulty of correctly treating these effects in polyatomic systems (in both cases the extent of ISC seems to be somewhat overestimated by theory[7,8,15,18]), detailed experimental results are required to validate theoretical predictions. In order to examine the effect of molecular complexity on product yields and ISC it is very interesting to move from acetylene to methylacetylene (propyne) and from ethylene to methylethylene (propene) because this permits us to explore how the reaction mechanism and dynamics change when replacing a H atom with a CH_3 group; in addition, these three C atom systems allow us to also address the effect of site addition of the O atom on the carbon chain of the hydrocarbon molecule. These reactions can be contrasted to the simpler $O(^3P) +$ acetylene and ethylene reactions.

In this paper we report a detailed synergic experimental and theoretical investigation on the dynamics of the reaction of $O(^3P)$ with propene where ISC can be at play. The reaction of $O(^3P)$ with propene, with respect to the simpler $O(^3P) + C_2H_4$ reaction, exhibits a much larger number of possible intermediates as well as product channels. Usually in this class of reactions there are several spin-allowed reaction channels which are thermodynamically open on the triplet PES, but ISC to the singlet PES can lead to the opening of further reaction channels in addition to those open on the triplet PES. Due to the larger structural complexity of the propene molecule compared to ethylene studied previously, this reaction can serve as a gateway to the richer chemical pathways available in larger hydrocarbons. The following nine reaction channels (with the enthalpy of formation at 0 K relative to reactants adopted from this work) are of relevance at the collision energy of about 10 kcal/mol

$$O(^3P) + CH_3CHCH_2 \rightarrow H + CH_3CHCHO \qquad \Delta H^0_0 = -17.2 \text{ kcal/mol} \qquad (1)$$

$$\rightarrow H + CH_3COCH_2 \qquad \Delta H^0_0 = -18.3 \text{ kcal/mol} \qquad (2)$$

$$\rightarrow CH_3CH_2 + HCO \qquad \Delta H^0_0 = -24.8 \text{ kcal/mol} \qquad (3)$$

$$\rightarrow CH_3 + CH_2CHO \qquad \Delta H^0_0 = -25.1 \text{ kcal/mol} \qquad (4)$$

$$\rightarrow CH_2CH_2 + H_2CO \qquad \Delta H^0_0 = -76.3 \text{ kcal/mol} \qquad (5)$$

$$\rightarrow {}^3CH_3CH + H_2CO \qquad \Delta H^0_0 = -5.4 \text{ kcal/mol} \qquad (6)$$

$$\rightarrow H_2 + CH_3CHCO \qquad \Delta H^0_0 = -78.8 \text{ kcal/mol} \qquad (7)$$

$$\rightarrow CH_2 + CH_3CHO \qquad \Delta H^0_0 = -10.7 \text{ kcal/mol} \qquad (8)$$

$$\rightarrow CH_2CHCH_2 + OH \qquad \Delta H^0_0 = -14.5 \text{ kcal/mol} \qquad (9)$$

Relevant questions are: (a) What is the fraction of terminal (C1) versus central (C2) carbon addition? (b) What are the primary products and on which spin-multiplicity PES are they

formed? (c) What is the extent of ISC? (d) How does ISC relate to the simpler O + acetylene and O + ethylene reactions? Answering all these questions is a very challenging task that cannot be fully addressed only experimentally. Support from high-level theory is needed to aid the interpretation of the experimental results and arrive to a detailed understanding of the reaction mechanism. A detailed understanding of this and similar reactive systems will facilitate the unraveling of the reaction mechanisms also in larger (four or more C atoms) alkynes and alkenes.

Therefore, to assist the interpretation of the experimental results, high-level electronic structure calculations have been performed on both triplet and singlet PES of the O(^{3}P) + propene reaction to determine stationary points, seams of triplet/singlet crossing, and related spin−orbit couplings. These properties are then used in nonadiabatic (within a Landau− Zener model) statistical RRKM/Master Equation calculations of product branching ratios, both at the collision energy of the CMB experiments and at room temperature, in order to compare the statistical predictions with also the recent kinetics results of Savee et al.[21]

One selected result of the present study, which highlights the importance of the ^{3}CH$_3$CH + H$_2$CO channel in the high energy conditions of the CMB experiments, has been recently published.[22] The present work complements and extends the previous paper, which was focused on the analysis of a single reaction channel and, from the computational standpoint, on the reactivity of the triplet PES.

1.1. Previous Work. From the kinetics standpoint, overall rate coefficients have been reported for the title reaction since the 1970s, and these have been refined over the years.[3,23] The total rate constant at room temperature has been determined to be $3.9 \pm 0.9 \times 10^{-12}$ cm^3 molecule^{-1} s^{-1}.[23] Early kinetics studies[24−26] (1964) reported formaldeyde, acetaldehyde, acetic acid, CO, and CO$_2$ as principal stable products and postulated channels 5 and 7 to be significant primary steps, but their quantitative relevance was questioned by later dynamics work by Kanofsky and Gutman[27] (1972). In fact, their pioneering crossed effusive molecular beam experiments employing fixed frequency photoionization with atomic resonance lamps revealed a variety of primary products being formed in this reaction. Major observable routes were found to be channels 3 and 4, while channels 5 and 6 were observed to be minor and channels 1, 2, and 7 apparently absent. Later studies by Blumenberg et al.[28] (1976) in low pressure reactors (crossed free jets and a laval nozzle reactor) using electron impact ionization mass spectrometric detection with tunable energy electrons (4.5−70 eV) confirmed that channels 3 and 4 are main channels, produced in comparable amounts (see Table 1). Notably, this latter study was able to detect both mass 30 (formaldehyde) (by distinguishing it from NO) and 28 (ethylene) (by distinguishing it from CO); however, channel 5 was deemed to be a minor route. Neither of the studies,[27,28] which correspond to a temperature of about 300 K, provided absolute branching ratios.

Koda et al.[29] (1991) using kinetics microwave absorption spectroscopy found the reaction produces a fraction of 0.29 ± 0.15 of vinoxy (CH$_2$CHO) (channel 4), which tends to increase with the decrease in pressure (see Table 1). Vinoxy formation was suggested to originate following the O attack to the terminal carbon atom of the C=C double bond and then ISC. The channel 3 HCO + C$_2$H$_5$ had a branching ratio of 1.39 ± 0.18 with respect to CH$_2$CHO + CH$_3$. In these studies the

Table 1. History of the Branching Ratios of the O(^{3}P) + C$_3$H$_6$ Reaction[a]

reaction channel	Kanofsky et al.[27] (1972)	Blumenberg et al.[28] (1977)	Koda et al.[29] (1991)	Knyazev et al.[30] (1992)	Washida et al.[31] (1998)	Quandt et al.[32] (1998)	Savee et al.[21] (2012) 300 K	this work EXPT E_c = 9.3 kcal mol^{-1}	this work RRKM E_c = 9.3 kcal mol^{-1}	this work RRKM[g] 300 K, 4 Torr
H + CH$_3$CHCHO	~0	-	-	0.46 ± 0.11	minor	-	0.46 ± 0.11[b] -	0.07 ± 0.02	0.261	0.159 (0.358)
H + CH$_3$COCH$_2$	~0	-	-		-	-	-	0.05 ± 0.02	0.010	0.003 (0.006)
H$_2$ + CH$_3$CHCO	~0	minor (<0.016)	-		-	-	0.014 ± 0.011 (0.05 ± 0.04)	0.03 ± 0.015	0.011[c]	0.018 (0.041)
CH$_3$ + CH$_2$CHO/CH$_3$CO	major	major (1.05)	[0.29 ± 0.15]	-	major	major	0.28 ± 0.07 (1.0)	0.32 ± 0.10	0.326	0.442 [0.249] (1.0)
C$_2$H$_5$ + HCO	major	major (1.0)	0.40 ± 0.05[e]	-	-	-	0.25 ± 0.07 (0.91 ± 0.30)	0.09 ± 0.04	0.070	0.283 (0.640)
^{3}CH$_3$CH + H$_2$CO	minor	minor (<0.05)	-	-	-	-		0.44 ± 0.15	0.321	0.065 (0.212)[f]
C$_2$H$_4$ + H$_2$CO							(0.27 ± 0.18)[d]		0	0

[a]The values between parentheses are the branching ratios relative to methyl + CH$_2$CHO/CH$_3$CO channel, while the values between square brackets are the absolute branching ratios of the CH$_3$ + CH$_2$CHO channel. [b]Taken from Knyazev et al.[30] in the reference work to determine absolute branching ratios.[21] [c]Includes H$_2$ from TS13 and TS16, which contribute equally to H$_2$ production. [d]Assigned as secondary product, potentially a primary product.[21] [e]Determined relatively to the rate of the CH$_3$ + CH$_2$CHO channel: 1.39 ± 0.18. [f]Includes C$_2$H$_4$ from TS16. [g]The branching ratio to the three-body C$_2$H$_4$ + H$_2$ + CO channel of 0.028 is not included in the Table.

ratio of the O(^{3}P) atom attacks to the C1 against the C2 could not be determined. It was noted that the primary HCO and CH$_2$CHO products react with other atomic and/or radical species at very high rates and that H$_2$CO (formaldehyde) is considered to be one of the main (secondary) products in the title reaction (as well as in any O(^{3}P) + olefin reaction). Knyazev et al.[30] (1992) studied the title reaction at room temperature under discharge flow conditions by resonance fluorescence spectroscopy of O and H atoms at pressures of 0.08–12 Torr. The branching ratio obtained for the channel producing H atoms was 0.46 ± 0.11 in all pressure ranges. However, it should be noted that in the same study the branching ratio of the H-forming channel in the related (reference) reaction O(^{3}P) + C$_2$H$_4$ was found to be 0.73 ± 0.04 at the lowest pressure of 1 Torr, while the established branching ratio of the H channel in O + ethylene at room temperature is 0.39 ± 0.10 (see ref 8).

Washida et al.[31] (1998) using laser-induced fluorescence (LIF) in a flow system observed CH$_2$CHO (+ CH$_3$) to be a major product from the title reaction. A weak fluorescence signal was attributed to 2-methylvinoxy from channel 1 CH$_3$CHCHO + H, considered to be a minor route. The isomeric channel 2 1-methylvinoxy + H was not observed.

Quandt et al.[32] (1998) also studied the title reaction by LIF under single-collision conditions and observed vinoxy formation. They also concluded that channel 4 (CH$_3$ + CH$_2$CHO) is necessarily a product of H atom migration on the singlet PES to form an energized aldehyde (propenal) which unimolecularly dissociates to a pair of radicals.

Very recently, Savee et al.[21] (2012) carried out state-of-the-art kinetics work employing time-resolved multiplexed photoionization mass spectrometry with tunable ultraviolet synchrotron radiation and provided both the rate coefficient and the product branching ratios for the O + propene reaction at 4 Torr and 298 K. Relative branching ratios of 1.00, 0.91 ± 0.30, and 0.05 ± 0.04 were reported for the primary product CH$_3$ + CH$_2$CHO (channel 4), C$_2$H$_5$ + HCO (channel 3), and H$_2$ + CH$_3$CHCO (channel 6) (see Table 1). The H$_2$CO + CH$_2$CH$_2$ channel 5 and CH$_2$ + CH$_3$CHO channel 7 were concluded to be secondary (or minor) reaction products, in this way not confirming the early conclusions[27,28] that channel 5, although deemed minor, was taking place. Notably, the H + C$_3$H$_5$O channels 1 and 2 were not observable for technical reasons in these kinetics experiments, so in order to provide an estimate of absolute branching fractions the yield of 0.46 ± 0.11 as determined by Knyazev et al.[30] was used for the H channel (see Table 1). The occurrence of some of the channels implies that triplet−singlet ISC is significant, but its extent could not be quantified.[21]

Ab initio quantum-mechanical calculations in several laboratories have provided triplet and singlet C$_3$H$_6$O PESs. While Zhang et al.[33] (2007) have explored only the triplet PES using UMP2 and QCSID calculations, De Boer & Dodd[34] (2007) have provided both triplet and singlet PESs using CBS-QB3 and G3 methods and have applied RRKM-based master equation calculations to derive statistical branching fractions on the adiabatic triplet and singlet PESs over the 300−3000 K temperature range and also as a function of pressure (0.001−760 Torr). While De Boer and Dodd[34] considered only the attack of the O atom to the C$_3$H$_6$ terminal olefinic carbon (C1), Zhang et al.[33] found that in the initial step the electrophilic O(^{3}P) atom attacks both carbon atoms (C1 and C2) of the double bond to form lower energy intermediates IM1

(^{3}CH$_3$CHCH$_2$O) and IM2 (^{3}CH$_3$COHCH$_2$) (see ref 33). Among the possible reaction channels formation of CH$_3$ + CH$_2$CHO (channel 4) from IM2 is predicted to be the dominant one, and the products CH$_3$COCH$_2$ + H (channel 2) from IM2 and CH$_3$CHCHO + H (channel 1) from IM1 are the secondary ones. Notably, the calculations indicate that the probability of initial addition of O(^{3}P) to C1 and C2 is about equal. Unfortunately, the recent kinetics results of Savee et al.[21] could not be compared with the adiabatic statistical results of Dodd and De Boer because the theoretical treatment did not include the possibility of intersystem crossing between triplet and singlet PESs. In addition, the level of theory is not expected to be sufficiently accurate for some of the product channels and related exit barriers, which, as will be shown in this work, have considerable multireference character.

In this paper, on the experimental front in order to investigate in deeper detail a multichannel nonadiabatic reaction such as O(^{3}P) + propene we have employed the CMB technique which (a) permits us to carry out investigations under truly single-collision conditions, avoiding the potential complications of a multiple-collision environment; (b) can verify unambiguously, on the basis of energy and linear momentum conservation, to which channel belongs a given product detected at a given m/z ratio; (c) can distinguish the possible isomeric products arising from H-elimination following the O atom attack on the terminal or central C atom of propene, provided they exhibit a different dynamics; (d) can exploit the extent of product recoil energy of a given channel to asses the presence or not of an exit potential barrier for that channel; (e) and, finally, can characterize the overall dynamics of the various competing product channels and rationalize them in terms of the underlying PES(s). On the theoretical front, we have carried out high-level *ab initio* calculations to establish as accurately as possible the relevant energetics (in particular barrier heights, isomerization paths, and seams of ISC); furthermore, statistical computation of branching ratios are performed that take into account also the possibility of ISC.

The paper is organized as follows. Section 2 gives the experimental and theoretical details. Section 3 presents the experimental results and their analysis. Section 4 describes the construction of the triplet/singlet reaction PESs and their analysis. The experimental and theoretical results are compared and discussed in Section 5. A summary and conclusions follow in Section 6. More extended theoretical details are given in the Supporting Information (SI).

2. METHODS

2.1. Experimental Section. The basics of our CMB apparatus have been described elsewhere,[35] while critical improvements, such as the soft electron-ionization capability, have been detailed recently.[4,36] Briefly, two supersonic beams of the reactants are crossed at 90° under single-collision conditions in a large scattering chamber kept at about 2 × 10^{-6} mbar under operating conditions. The angular and velocity distributions of the reaction products are recorded by a triply differentially pumped, ultrahigh-vacuum (UHV) (10^{-11} mbar) detector equipped with a tunable electron impact ionizer followed by a quadrupole mass filter and an off-axis electron multiplier. The whole detector unit can be rotated in the plane of the two beams around their intersection axis (Θ = 0° represents the direction of the atomic oxygen beam). The velocity of reactants and products is derived using single-shot and pseudorandom, respectively, TOF analysis. The supersonic

beam of O atoms was produced by means of a radio frequency (RF) discharge source[37,38] (based on the design of Sibener et al.[39]) operating at an RF power of 300 W and a pressure of 145 mbar of a dilute (5%) mixture of O_2 in He carrier gas through a 0.28 mm diameter quartz nozzle; peak velocity and speed ratio were 2481 m/s and 5.2, respectively. We wish to emphasize here that central for the success of the present CMB studies has been the excellent performance of our high-intensity supersonic atomic oxygen nozzle beam RF source which follows the very successful design and implementation of Sibener et al.[39] The supersonic beam of propene was generated by expanding through a 100 μm diameter stainless-steel nozzle kept at room temperature under 390 mbar of neat propene. Beam peak velocity and speed ratio were 740 m/s and 4.0, respectively. The resulting collision energy was 9.3 kcal mol^{-1}. The very small percentage ($\leq$5%, as obtained from magnetic analysis of the beam[37]) of O(^{1}D) present in the atomic oxygen beam is expected to contribute negligibly to the results because the reactivity of O(^{3}P) (dominant in the beam) becomes comparable to that of O(^{1}D) at this high collision energy, and presumably, as for the case of the reaction O + C_2H_2,[6] the O(^{1}D) reaction mainly produces OH + C_3H_5.

In the study of the O(^{3}P) + C_3H_6 reaction with the CMB technique it is very easy to detect the heavy products corresponding to channels 1, 2, and 7, because C_3H_5O and C_3H_4O products are kinematically constrained in a narrow angular region around the center-of-mass (see Section 3 and Figure 1). The detection of any of the two coproducts from the C−C bond-breaking channels is much more problematic because of the dissociative ionization of the elastically/
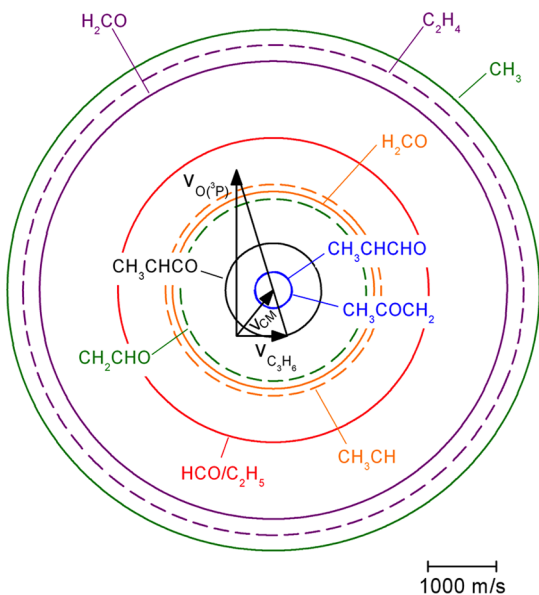
Figure 1. Velocity vector (Newton) diagram showing the circles that delimit the angular range and center-of-mass speed for the products of the various channels of the reaction O(^{3}P) + propene at E_c = 9.3 kcal/mol. Blue continuous/dashed lines: Newton circles for the H-displacement channels leading to CH_3CHCHO/CH_3COCH_2 (indistinguishable in the figure). Black continuous line: Newton circle for CH_3CHCO. Olive green continuous/dashed line: Newton circles for CH_3/CH_2CHO. Red line: Newton circle for both HCO and C_2H_5; the two circles are identical because HCO and C_2H_5 have the same mass. Purple continuous/dashed lines: Newton circle for H_2CO/C_2H_4. Orange continuous/dashed line: Newton circle for H_2CO/$^3CH_3CH$.

inelastically scattered propene reactant beam. In particular, detection of C_2H_4 is also plagued by the high inherent detector background at m/z = 28 due to residual CO in any UHV chamber. The product laboratory (LAB) angular distributions, $N(\Theta)$, were recorded at m/z = 56 (C_3H_4O) and 55 (C_3H_3O) using 60 and 17 eV electron energy, while those at m/z = 29 (HCO and C_2H_5) and 15 (CH$_3$) only at 17 eV by counting for 50 or 100 s at each angle and averaging over at least five scans; the C_3H_6 beam was modulated at 160 Hz by a tuning-fork chopper for background subtraction. TOF data were recorded at the center-of-mass (CM) angle, Θ_{CM}, of 38°, besides at m/z = 56, 55, 29, and 15, also at m/z = 30 and 28 (for m/z = 55 and 29 also at Θ = 26° and 50°) with counting times ranging from 1 to 4 h depending upon product mass and signal intensity, using the cross-correlation TOF technique with four 127-bit pseudorandom sequences. High-time resolution was achieved by spinning the pseudorandom TOF disk, located at the entrance of the detector, at 328.1 Hz corresponding to a dwell time of 6 μs/channel. The flight length was 24.3 cm.

In a CMB experiment with mass spectrometric/TOF detection the laboratory angular distribution, $N(\Theta)$, and the product intensity as a function of the scattering angle Θ and arrival time t, what we call the time-of-flight spectrum, $N(\Theta, t)$, are measured in the LAB system of coordinates, but for the physical interpretation of the scattering data it is necessary to perform a coordinate transformation and move to the CM reference frame.[40,41] It can be easily demonstrated[40] that, for each reaction channel, the relation between LAB and CM product flux is given by $I_{LAB}(\Theta,v) = I_{CM}(\theta,u)v^2/u^2$, where Θ and v are the LAB scattering angle and velocity, respectively, while θ and u are the corresponding CM quantities. Since the EI mass-spectrometric detector measures the number density of products, $N(\Theta)$, rather than the flux, the actual relation between the LAB density and the CM flux is given by

$$N_{LAB}(\Theta, v) = I_{CM}(\theta, u)v/u^2 \qquad (10)$$

Because of the finite resolution of experimental conditions (angular and velocity spread of the reactant beams and angular resolution of the detector), the LAB to CM transformation is not single-valued, and therefore, analysis of the laboratory data is usually performed by forward convoluting tentative CM distributions over the experimental conditions. In other words, the CM angular and velocity distributions are assumed, averaged, and transformed to the LAB frame for comparison with the experimental distributions, and the procedure is repeated until a satisfactory fit of the experimental distributions is obtained. The final outcome of a reactive scattering experiment is the generation of a velocity-flux contour map of the reaction products for each channel, i.e., the plot of intensity as a function of angle and velocity in the CM system, $I_{CM}(\theta, u)$. The differential cross section $I_{CM}(\theta, u)$ is commonly factorized into the product of the velocity (or translational energy) distribution, $P(u)$ (or $P(E'_T)$), and the angular distribution, $T(\theta)$: $I_{CM}(\theta, E'_T) = T(\theta)P(E'_T)$. In some cases the coupling between the $T(\theta)$ and $P(E'_T)$ functions needs to be accounted for, but it was not found (within our sensitivity) in the present study. The $T(\theta)$ and $P(E'_T)$ functions contain all the information about the dynamics.

For reaction with multiple channels, as is the case in the present work, if more than one product channel contributes to a given m/z ratio, a weighted total CM differential cross section reflecting the various possible contributions is used in the data

analysis of the LAB angular and TOF distributions for a specific m/z, that is

$$I_{CM}(\theta, E'_T)_{total} = \sum_i w_i \times [T(\theta) \times P(E'_T)]_i \quad (11)$$

with the parameter w_i representing the relative contribution of the integral cross section of the ith channel, being a best-fit parameter.[4,6,36]

2.2. Theoretical. The structure and energy of stationary points on the potential energy surface were determined at the CASPT2 level[42,43] using the aug-cc-pVTZ basis set.[44] Different active spaces were considered depending on the reaction channel under study, as is described in the Results section and reported in detail in the Supporting Information to this paper. As a general rule, a smaller active space was used to determine structures, while energies were computed extending systematically the active space until convergence was reached. CASPT2 energy barriers were computed relatively to the products for reactions with small energy barriers and to the reactant in the other case using the same active space. Vibrational frequencies were determined at the CASPT2 level with the same active space used to optimize the structure. All wells are characterized by the absence of imaginary vibrational frequencies and all transition states by a single imaginary frequency. When the T1 diagnostic was smaller than 0.02 or near this value, which is usually considered to be indicative of multireference character, energies were also computed on geometries determined at the CASPT2 level using unrestricted CCSD(T) theory with the aug-cc-pVDZ and the aug-cc-pVTZ basis sets. This was for example the case for all the energy wells. The scheme proposed by Martin[45] was then used to extrapolate the energies to the complete basis set limit. All calculations were performed using the Molpro 2008 suite of programs.[46]

The dynamic evolution over the C_3H_6O PES was studied integrating the 1-dimensional Master Equation using RRKM microcanonical rate constants.[47,48] RRKM rates $k(E,J)$ were determined as a function of energy E and angular momentum J using the density of states convoluted over all external rotational and vibrational degrees of freedom at E and J steps of 1 cm^{-1}. In particular RRKM rate constants for reactions with a loose transition state were calculated with E, J resolved microcanonical variational transition state theory. The $k(E,J)$ so evaluated were successively averaged over J as suggested by Miller et al.[49] and lumped into energy bins with size of 50 cm^{-1}. The master equation was integrated using our RRKM/master equation stochastic code.[47] The degeneration of low vibrational frequencies of torsional modes into hindered rotors was explicitly considered in the evaluation of kinetic constants by direct analysis of the rotational PES. When the internal rotation was hindered by small energy barriers the corresponding density of states was calculated by direct count of the quantized energy levels obtained solving the Schrödinger equation for a 1D rotor on a PES determined at the CASPT2/cc-pVDZ level, as described in previous works.[50] It was found that most wells and transition states possess one hindered rotor, corresponding to methyl rotation, while in a few cases a second hindered rotor is present. In these cases the two hindered rotors were treated independently, and the calculated density of states was convoluted. The electronic partition function of oxygen was computed accounting explicitly for the population and degeneracy of the three lowest electronic states as a function of temperature. The contribution of quantum tunneling was included for all reactions with imaginary vibrational frequency

larger than 1300i cm^{-1} adopting the Eckart model for tunneling over asymmetric barriers.[51] Decomposition to reactants is explicitly considered, and it is in competition with the other possible reaction channels. Two different sets of simulations were performed, the first corresponding to the present CMB study and the second to the 298 K−4 Torr multiplexed photoionization mass spectrometry study of Savee et al.[21] Addition to the terminal and central carbon of propene was considered as different events, thus described by two distinct PESs and requiring two different RRKM/ME simulations. The initial energy of the entrance wells was determined stochastically from the normalized product of the reactants' rovibrational density of states and the microcanonical rate constants for the two bimolecular entrance channels $k_{add}(E)$, determined applying microscopic reversibility from the corresponding dissociation reaction $k_{dec}(E)$ assuming that propene has a 300 K Boltzmann internal (vibrational) energy (the exact expression is reported in Cavallotti et al.[52]). The relative weight of the two entrance channels was assumed to be equal to that of the 300 K rate constants for both sets of simulation. The kinetic energy of the CMB experiment was added to the energy of the entrance well determined stochastically. The collisional energy transfer for the thermal simulations was modeled adopting an exponential down model using a T-dependent ΔE_{down} value of $200 \times (T/298)^{0.875}$, which was used with success to model similar systems.[53]

The intersystem crossing rate was computed using Landau−Zener theory[54] implemented as suggested by Harvey,[55] suggested by Polino et al.,[56] and described in detail in our recent study.[22]

3. EXPERIMENTAL RESULTS AND ANALYSIS

3.1. Product Angular and Velocity Distributions in the LAB Frame. Before presenting and discussing the experimental results it is useful to illustrate the velocity vector diagram of the system which depicts the kinematics of the reaction and how the different possible products can be scattered in angle and velocity with respect to the center-of-mass.

The most probable velocity vector (or so-called "Newton") diagram showing the kinematics of the various channels for the O + propene reaction is reported in Figure 1. It can be easily appreciated that the H-displacement channels (1 and 2) are those with the most favorable kinematics: in fact, the heavy coproducts C_3H_5O are confined into much smaller Newton cicles compared to those associated with the C−C bond-breaking channels where, because two cofragments of comparable mass are produced, on the basis of linear momentum conservation the products are scattered over a very wide Newton circle. Since the solid angle subtended by the detector is always the same and so is the detector distance from the collision center, the signal recorded for the H-displacement channel(s) by detecting the heavy coproduct, because of its low CM velocity (see eq 10), will appear to be prominent in the LAB reference frame for comparable reaction cross sections of the various channels.

Reactive signals were detected at m/z = 57 (C_3H_5O), 56 (C_3H_4O), 55 (C_3H_3O), 30 (H_2CO), 29 (HCO and C_2H_5), 28 (C_2H_4), and 15 (CH_3). The signal at m/z = 57 would correspond to the parent ion of possible C_3H_5O products from H displacement channels 1 and 2; however, its intensity is very weak, corresponding roughly to about 3% of the total signal attributed to the H channels: this indicates that it is all due to ^{13}C natural isotopic abundance, and therefore we conclude that

the parent ion of C_3H_5O is not stable, even upon soft ionization by 17 eV electron energy. This confirms the finding of recent kinetics work where the parent ion of C_3H_5O was not observed with soft photoionization energy of 10 eV.[21] A similar situation was encountered when trying to detect the vinoxy radical produced from the $O(^3P)$ + ethylene reaction, both with soft electron-ionization and soft photoionization by synchrotron radiation (only below 12 eV some parent ions become detectable[4,5]). Notably, while the fact that CH_3CHCHO (methylvinoxy) does not give a parent ion upon ionization is a problem in kinetics studies with soft photoionization,[21] it does not represent a complication in CMB experiments because from angular and velocity distribution measurements, on the basis on energy and linear momentum conservation,[40] it is possible to attribute unambiguously the m/z = 56 and 55 daughter ion signals to the product C_3H_5O (mass 57) coming from the H elimination channel(s). It should be noted that the signals at m/z = 56 and 55 (m/z = 54 was negligible) can partly originate from daughter ions of the H channel products and part from the parent (m/z = 56) or daughter ions (m/z = 55) of the H_2 channel (7). Again, on the basis of energy and momentum conservation it is possible to disentangle the various contributions (see below).

In Figure 2 are reported comparatively the LAB angular distributions measured at m/z = 56, 55, 29, and 15. The TOF distributions recorded at the center-of-mass angle, Θ_{CM}, of 38° for the six masses 56, 55, 30, 29, 28, and 15 are shown in Figure 3. It should be noted that angular distributions were measured only at m/z = 56, 55, 29, and 15 because the S/N at m/z = 30 and 28 was too low due to the high background at these masses (especially at mass 28). Figures 4 and 5 show the TOF spectra at m/z = 55 and m/z = 29, respectively, at three different laboratory angles (the CM angle and 26° and 50°, corresponding to the forward and backward direction, respectively). The distributions at m/z = 56 and 55 shown in Figures 2 and 3 were obtained by using an ionizing electron energy of 60 eV, but data were taken also at 17 eV for normalization purposes and also to explore further the differences attributable to the two isomeric H elimination channels 1 and 2 (see below). On the contrary, to measure product angular and TOF distributions at m/z of 30, 29, 28 and 15, we took full advantage of the soft EI technique, as these distributions could be measured only if reducing the background signal and interferences from dissociative ionization processes by employing 17 eV electron energy. Notably, operating with essentially zero background at 17 eV, no signal was detected at m/z = 14 and 17, which rules out (within our sensitivity, i.e., BR ≤ 1−2%) the weakly exoergic channel 8 and also the H abstraction pathway leading to OH formation (which although it is exoergic by 14.5 kcal mol⁻¹ has a high entrance barrier of about 5 kcal/mol above the reactant asymptote).

As can be seen from Figure 2 (top two panels) the angular distributions at m/z = 56 and 55 are fairly narrow and peak around the CM angle, reflecting mainly the H elimination channels; at the same time, the corresponding TOF spectra (see top two panels in Figure 3) are slow and centered around the CM velocity. In contrast, as Figures 2 and 3 show, in the angular distributions at m/z = 29 and 15 there is intensity extending beyond the Newton circles amenable to the H/H_2 channels (see Figure 1), and in the TOF distributions at m/z = 30, 29, 28, and 15 there is intensity also at velocities much larger (i.e., at fight times much shorter) than that of the center-
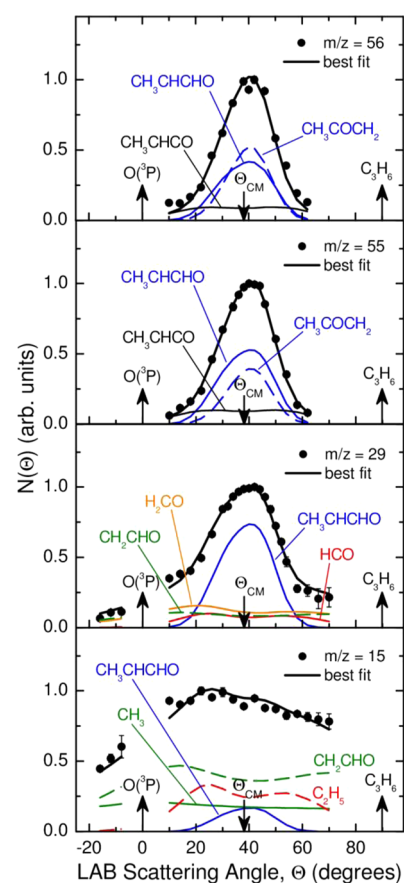
Figure 2. LAB angular distributions at m/z = 56, 55, 29, and 15 for the $O(^3P)$ + propene reaction at E_c = 9.3 kcal mol⁻¹. The solid black curves represent the calculated distributions when using the best-fit CM functions of Figure 6 (see text). The separate contributions to the calculated global LAB angular distributions are indicated with the formula of the corresponding product (color and symbol coding as in Figure 1).

of-mass around which the C_3H_5O/C_3H_4O products are peaked. Notably, at these lower masses, especially at m/z = 29 and 28, there is still a significant contribution arising from the dissociative ionization of the C_3H_5O products, despite the low ionization energy of 17 eV. Clearly the angular distributions at m/z = 29 and 15 are quite different from those at m/z = 56/55, thus implying different reactive signal sources, which are disentangled by TOF measurements. Although the m/z = 56 and 55 TOF spectra are clearly unimodal (see two top panels in Figures 3 and 4), they are somewhat different indicating that at least two product channels with different dynamics are contributing to the signal at these masses (see below). In contrast, the TOF spectra at the other masses (see Figures 3 and 5) have a pronounced structure with two or three peaks.
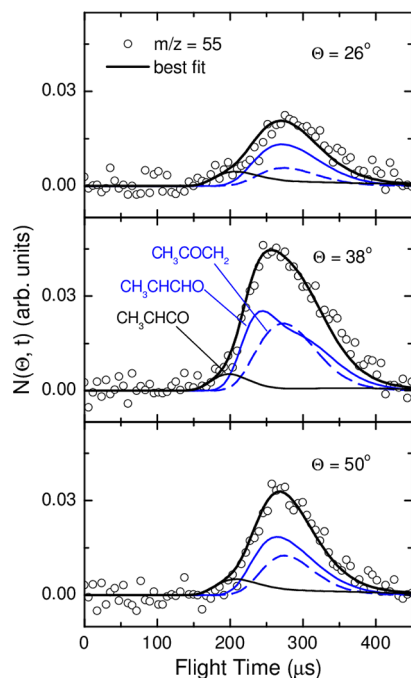
Quantitative information is obtained by moving from the LAB coordinate system to the CM one and analyzing the product angular, $T(\theta)$, and translational energy, $P(E'_T)$, distributions into which the CM product flux can be factorized (the best-fit CM functions are actually derived by a forward convolution fit of the product LAB angular and TOF distributions; see Section 2). The solid curves superimposed on the experimental results in the Figures 2−5 are the calculated curves when using the best-fit CM functions reported in Figure 6. To reach a good fit of the data it was necessary to consider multiple contributions associated with
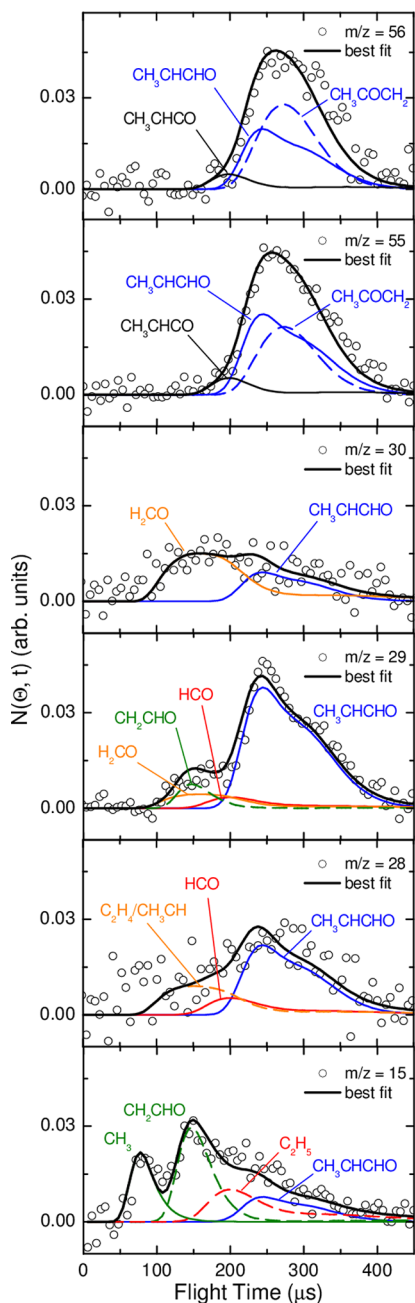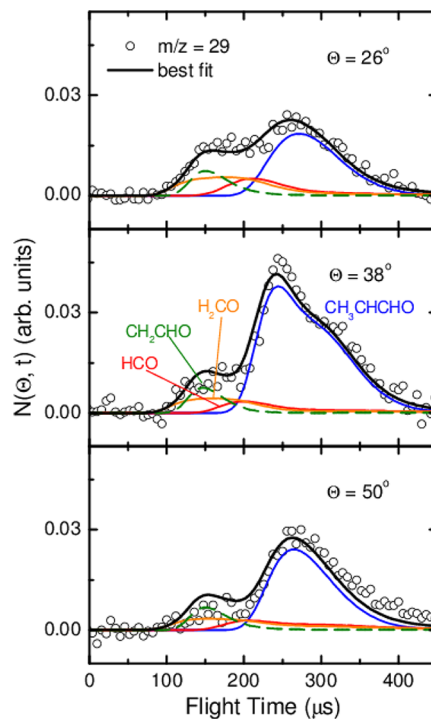
Figure 3. Time-of-flight distributions at $m/z = 56, 55, 30, 29, 28,$ and 15 recorded at Θ_{CM} (= 38°). Symbols as in Figure 2.
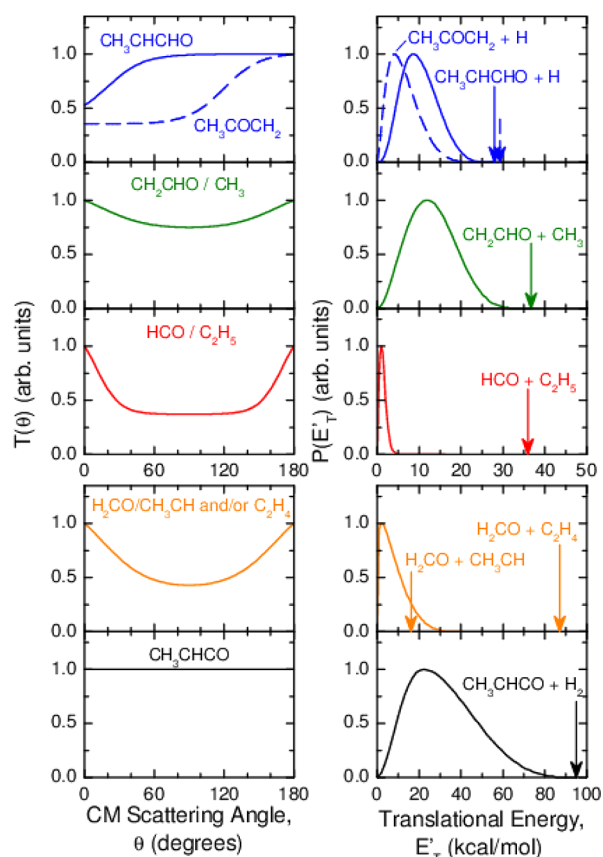

Figure 4. Time-of-flight distributions at $m/z = 55$ recorded at the three indicated LAB angles. Symbols as in Figures 2 and 3.

Figure 5. Time-of-flight distributions at $m/z = 29$ recorded at the three indicated LAB angles. Symbols as in the Figures 2, 3, and 4.

each product contributing at the signal for that m/z (see below), according to eq 11 (see Section 2).

3.2. $m/z = 56$ and 55 Data: H and H_2 Elimination Channels. From angular and TOF measurements at $m/z = 56$ and 55 (and also at daughter ion 29) we have characterized the occurrence of the H-displacement channels 1 and 2 leading to the two isomeric species CH_3CHCHO and CH_3COCH_2 and the H_2 elimination channel 7. In fact, in order to fit the wings of the angular distributions and the fast shoulder of the TOF spectra at $m/z = 56$ and 55 (see top two panels in Figures 2 and 3 and also Figure 4) we needed to invoke the occurrence of the strongly exoergic (by about 80 kcal/mol) H_2 elimination channel 7. At the same time, to fit simultaneously the main part of the angular and TOF distributions at the two masses we needed to invoke the contributions of two dynamically different

H elimination channels (channels 1 and 2), with different relative weights at $m/z = 56$ and 55. As can be seen at $m/z = 55$ the relative contribution of the CH_3COCH_2 isomer is narrower (reflecting a smaller average fraction of energy in product translation ($\langle f_T \rangle = 0.22$) (see Figure 6, top right panel) and less intense than the contribution from the CH_3CHCHO isomer which is characterized by more energy in translation ($\langle f_T \rangle = 0.37$) (see Figure 6, top right panel). The average product
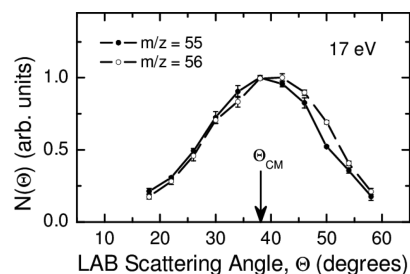
at these two masses should be somewhat different: indeed, as Figure 7 clearly shows, the two experimental angular
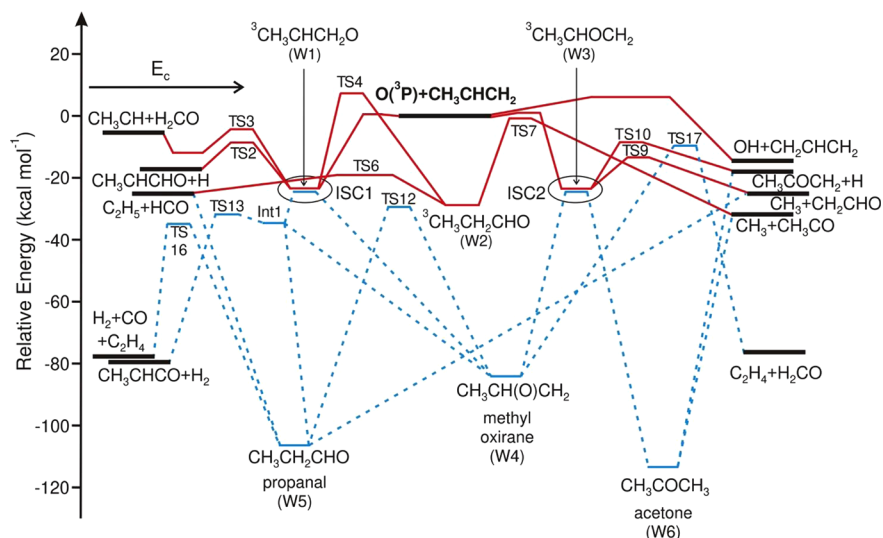

Figure 7. LAB angular distributions at $m/z = 56$ and 55 measured at 17 eV electron energy. The lines through the data points are only to guide the eye.

distributions (measured at 17 electron energy with small error bars) are somewhat different, with that at $m/z = 56$ being somewhat more backward shifted with respect to that at $m/z = 55$. This indicates that the more backward peaked CH_3COCH_2 isomer fragments more to mass 56 than to mass 55 with respect to the less backward peaked CH_3CHCHO isomer (see Figure 6, top panel lhs). As will be discussed below, the H elimination channels leading to radical products occur on the triplet PES, while the H_2 elimination channel leading to molecular products occurs on the singlet PES following ISC. In fact, the methylketene product from the strongly exoergic H_2 elimination channel exhibits a symmetric (isotropic) CM angular distribution (see bottom left panel in Figure 6), i.e., a different dynamics (via a long-lived complex mechanism), with an extended $P(E'_T)$ peaking at about 25 kcal mol^{-1} and reflecting a large fraction of energy released in translation, $\langle f_T \rangle$ = 0.33 (see bottom right panel in Figure 6).

3.3. m/z = **30, 29, 28, and 15 Data: The C−C Bond-Breaking Channels** $CH_3 + CH_2CHO$**,** $C_2H_5 + HCO$**, and** $C_2H_4/^3CH_3CH + H_2CO$**.** Besides the parent ion of the CH_3 product from channel 4, numerous other possible products can contribute via fragmentation to $m/z = 15$: these are CH_2CHO (vinoxy), the counter-fragment of CH_3; CH_3CHCHO (methylvinoxy) from channel 1; and C_2H_5 (from channel 3). The relative contributions from channels 4, 1, and 3 to the angular distribution at $m/z = 15$ (see Figure 2, bottom panel) are disentangled from TOF measurements (see Figure 3, bottom panel) in which the parent ion of the methyl radical product and its counter-fragment vinoxy (CH_2CHO) appear as two well-resolved fast peaks. It should be noted that the TOF peak of the contribution associated with CH_3 is much faster than that associated with CH_2CHO because the lighter coproduct is produced with a much higher speed on the basis of linear momentum conservation (the two coproducts are momentum-matched) (see Newton diagram of Figure 1); in contrast, the fragment ion from the H channel 1 appears on the slow tail of the spectrum, while the remaining intensity between CH_2CHO and CH_3CHCHO is attributed to the C_2H_5 product formed in channel 3 with little recoil energy.

According to our analysis at $m/z = 29$ (see Figures 2, 3, and 5) we have a contribution from H_2CO (which is known to strongly fragment to daughter ion HCO$^+$) from channel 5 and/ or 6, from the parent ion of the formyl radical produced in channel 3 and from CH_2CHO (which is known to fragment to HCO$^+$) formed in channel 4. The CM functions of the H_2CO (channels 5 and/or 6) and C_2H_4/CH_3CH coproducts are

Figure 6. (Left-hand side): Best-fit CM angular distributions for the products CH_3CHCHO (blue solid line), CH_3COCH_2 (blue dashed line), CH_2CHO/CH_3 (olive green line), HCO/C_2H_5 (red line), H_2CO/CH_3CH (C_2H_4) (orange line), and CH_3CHCO (black line). (Right-hand side): Best-fit CM product translational energy distributions. Symbols as in lhs panel. The total energy available to the products is indicated by an arrow.

translational energy $\langle E'_T \rangle$ is defined as $\langle E'_T \rangle = \sum P(E'_T)E'_T / \sum P(E'_T)$, and the average fraction of total available energy E_{TOT} ($E_{TOT} = E_c - \Delta H^0_0$) channelled into translation, $\langle f_T \rangle$, is defined as $\langle f_T \rangle = \langle E'_T \rangle / E_{TOT}$.

The fact that the $P(E'_T)$ distribution of $CH_3CHCHO + H$ peaks away from zero determines a slight bimodality in the corresponding contribution to the TOF spectra at $m/z = 56$ and 55 and also to that at $m/z = 29$, to which it is the CH_3CHCHO isomer which essentially contributes via dissociative ionization (that is, CH_3CHCHO fragments strongly to HCO$^+$, while the isomer CH_3COCH_2 does it negligibly). In other words, the signal at $m/z = 56$ reflects some parent ion of the CH_3CHCO (methylketene) product (from the H_2 elimination channel 7) and some daughter ions from CH_3CHCHO/CH_3COCH_2 isomers (from the two H elimination channels 1 and 2). In turn, the signal at $m/z = 55$ reflects also daughter ions of the CH_3CHCO product and daughter ions from the two C_3H_5O isomers but in different ratio than at $m/z = 56$, as the relative best-fit contributions at the two different masses clearly indicate (see Figures 2 and 3, top two panels). As can be seen from Figure 6 (top left panel) the CM angular distribution of CH_3CHCHO is nearly isotropic with a backward bias, while that of the CH_3COCH_2 isomer is more strongly backward peaked. Because the two C_3H_5O isomers fragment differently at $m/z = 56$ and 55 and exhibit a different extent of backward scattering, the overall angular distributions

Figure 8. Potential energy diagram illustrating stationary points on the triplet (solid lines) and singlet (dashed lines) C₃H₆O PESs. Structures and vibrational frequencies were computed at the CASPT/aug-cc-pVTZ level using the active spaces reported in Table S3 (SI). Energies were computed at the CCSD(T)/CBS level, but an exception was made for reactions with multireference character, in which case are reported CASPT2 energies calculated with extended active spaces. Only the main observed pathways are illustrated in this simplified version of the PESs (see Figures S1 and S2 (SI) for more detailed PESs). Pathways for both terminal (lhs) and central (rhs) addition of O(³P) to C₃H₆ are illustrated. The two seams of ISC are indicated. The energy scale is relative to the energy of the reactants at 0 K and includes ZPE corrections.

confirmed from TOF measurements at the parent ion ($m/z = 30$) of H_2CO which was observed together with some daughter ions of the H channel 1 and at the parent ion ($m/z = 28$) of the fast C_2H_4/CH_3CH product (channels 5 and/or 6) which was observed together with some contribution from daughter ions of HCO and CH_3CHCHO products from channel 3 and 1, respectively (see Figure 3, third and fifth panel, respectively, from top).

3.4. Product Angular and Translational Energy Distributions in the CM System. As can be seen from the best-fit CM functions associated with the various channels shown in Figure 6, with the exception of the $T(\theta)$ associated with the two C_3H_5O isomer products and discussed above, all the other $T(\theta)$'s are backward−forward symmetric with a varying degree of polarization, ranging from isotropic for methylketene to significantly polarized for HCO/C_2H_5 and also H_2CO. In all cases, except the H channels, the intensity distributed in the entire 0°−180° angular range is consistent with the formation of one or more long-lived complexes (i.e., living many rotational periods—more than 5 to 6 according to the "osculating complex" model for chemical reactions[57,58]), and this is consistent with the present statistical calculations of intermediate lifetimes (see Section 5.3).

The product translational energy distributions, $P(E'_T)$'s (Figure 6, right-hand side), exhibit a quite different shape for each channel, implying that they experience different parts of the PES. In the H-displacement channel where the structureless H atom is formed, the $P(E'_T)$ for channel 1 and channel 2 peaks at 8.3 and 3.6 kcal mol⁻¹, respectively, and the corresponding average fractions of available energy released as product translational energy, $\langle f_T \rangle$, are 0.38 and 0.23. Also for the $CH_3 + CH_2CHO$ channel the $P(E'_T)$ is quite energetic, peaking at about 12 kcal mol⁻¹ and corresponding to $\langle f_T \rangle = 0.38$. These large fractions of energy released in translation reflect significant exit potential barriers, as is found in the calculated triplet PES for all exit channels. In contrast, the $P(E'_T)$ for channel 3 (leading to $HCO + C_2H_5$) peaks at nearly

zero and extends to only 5 kcal mol⁻¹ corresponding to a very small fraction (0.04) of energy released in translation; this reflects the barrierless dissociation of singlet propanal to two radical products with very large internal excitation. The $P(E'_T)$ for the H_2CO channel(s) peaks at 2.4 kcal/mol and extends up to about 30 kcal/mol, with an average fraction of energy in translation of 8.2 kcal/mol. Considering that the exoergicity of channel 6 (leading to ³CH₃CH + H₂CO) is 5.4 kcal/mol, the derived $P(E'_T)$ extends beyond the limit of energy conservation for this triplet channel; this is an indication that some H_2CO is also formed from the singlet PES, where the exoergicity of channel 5 (leading to $C_2H_4 + H_2CO$) is 76 kcal/mol. Unfortunately the resolution of our experiment does not allow us to disentangle unambiguously the triplet and singlet relative contributions to formaldehyde formation. Finally, the $P(E'_T)$ of channel 7 (leading to $CH_3CHCO + H_2$) peaks at 22.4 kcal/mol and corresponds to a high fraction ($\langle f_T \rangle = 0.35$) of energy in translation, and this reflects a high exit potential barrier on the singlet PES for H_2 elimination.

3.5. Branching Ratios. Following the procedure outlined by Schmoltner et al.[16] (recently applied also to the reactions $O(^3P) + C_2H_2$ and $O(^3P) + C_2H_4$,[6,8] from our experimental data, once the origin of the various ion signals is sorted out, the relative yield of each product can be derived from the relative apparent cross section (obtained from the best fit analysis of the LAB data), the estimated ionization cross section, and the measured total ion yield for a specific product, taking into account the quadrupole transmission. The experimentally derived branching ratios, which have uncertainties ranging from ±20% to ±50% depending on the channel, are reported in Table 1, where they are compared with the previous (partial) determinations from various types of flow studies at room temperature, as well as with the present statistical RRKM/ME results (see Section 5.3). For a detailed discussion on how branching ratios are derived in these CMB studies and what the sources of uncertainties are, the reader can refer, for instance, to Section IV of ref 6 and Section V.A.6 of ref 8 where the cases of

O + C_2H_2 and O + C_2H_4 are discussed in detail. As discussed there, the ionization cross sections at their maximum (70 eV) have been evaluated using the procedure of Fitch and Sauter,[59] which is based on the additivity of atomic ionization cross sections. Their value at the electron energy of 17 eV is estimated using the total ionization cross section curves measured at the various m/z values as a function of electron energy; although this is an approximate procedure, it seems to work satisfactorily, leading presumably to uncertainties which are within the larger uncertainties of the overall procedure, which depending on signal intensities can be as large as 50% as quoted above.

4. CONSTRUCTION AND ANALYSIS OF THE O(^{3}P) + C_3H_6 PES

The PES used in the study of the reactivity between O(^{3}P) and propene was constructed on the basis of previous computational investigations of the singlet and triplet C_3H_6O PES[33,34] and of the C_2H_4O PES,[7,15,20] which were complemented by an additional search for new possible reaction channels. The most important reactive features of this system are the kinetics of the two entrance channels, the reactivity on the triplet PES, the determination of the ISC rates, and the reactivity on the singlet PES, which are all described in detail in the following. A synthesis of the PESs resulting from the present calculations is shown in Figure 8, where we highlight the main triplet and singlet reaction intermediates and reaction pathways (see below and the SI for further details). The full singlet and triplet PESs used in the ME simulations are reported in Figures S1 and S2 (SI).

4.1. Reactivity on the Triplet PES. The reactivity on the triplet PES as well as the estimation of the ISC rate are described in detail in our previous publication[22] and in its Supporting Information, and it will therefore be only briefly described here. Oxygen atoms can directly react with propene to give addition to the two unsaturated carbon atoms and hydrogen abstraction from the methyl group. Other abstraction reactions are possible but are expected to proceed at a much lower rate. In the case of addition, the two transition states are connected on the reactant side to the same precursor complex, lying about 1.9 kcal/mol below the reactant energy. The presence of a precursor complex is indicative of the existence of two distinct transition states, an inner and an outer transition state, with the first one controlling the rate fluxes in the investigated conditions. The approach used to locate the transition states of the addition reactions is similar to the one adopted by Sabbah et al.[23] and is described in detail in our recent publication.[22] The calculated activation energies for addition to the terminal and central carbon used in the RRKM/ME simulations, determined at the CASPT(10e,9o) level using the aug-cc-pVTZ basis set, are 0.16 kcal/mol for addition to the terminal carbon and 0.45 kcal/mol for addition to the central carbon. The energy barrier for H abstraction from the CH_3 group of propene is 4.4 kcal/mol, calculated at the CASPT/aug-cc-pVTZ level using a (8e,7o) active space and state averaging the CAS simulations over two states. The high-pressure rate constant for the reaction of O(^{3}P) with propene can be computed summing the rate of the addition and abstraction reactions (the rate constants interpolated between 300 and 2000 K are reported in Table S2, SI). The calculated total rate constants are in good agreement with experimental measurements in the investigated temperature range, as shown in our recent work (see Figure 5 in ref 22). In particular at 300

K the calculated reaction rate, 4.7×10^{-12} cm^3/molecule/s, is in very good agreement with the recent measurement of $3.9 \pm 0.9 \times 10^{-12}$ cm^3/molecule/s performed by Sabbah et al.[23] using the CRESU technique. The present results confirm that at 300 K oxygen addition to the terminal C is the dominant process, as predicted by Cvetanovic,[25,26] though addition to the central C is not negligible as it accounts for about 30% of the total rate. As the temperature rises H abstraction becomes a competitive reaction channel, though it is not relevant in the experimental conditions investigated in the present study. The rate constant calculated for H abstraction is about a factor of 2 faster than the value determined by Tsang[60] on the basis of analogy rules for abstraction from allylic hydrogen atoms.

The addition of O(^{3}P) to the terminal carbon atom is exothermic by 23.7 kcal/mol and leads to the formation of a CH_3CHCH_2O biradical species (W1) that can follow several reaction routes (see Figure 8): H transfer to the central carbon to form the triplet state of propanal (W2), H loss from the CH_2O group via TS2, decomposition to the $^3CH_3CH$ biradical + H_2CO via TS3, and intersystem crossing (ISC1) to the singlet PES. The energy barriers calculated at the CASPT2 and CCSD(T)/CBS level for the H transfer and H dissociation reactions are similar, indicating that for these reactions multireference effects play a minor role (see Tables S5 and S6, SI), while this is not the case for decomposition to $^3CH_3CH$ + formaldehyde and for ISC crossing, in which case the barrier heights were determined at the CASPT2 level. Because of the high energy barrier H transfer is not competitive with the other three processes in the investigated temperature range, so that its contribution to the overall system reactivity is negligible. Though some test simulations showed that its relative weight increases with temperature, it still remains a minor channel for this system. Following hydrogen transfer, the main reaction route is decomposition to the ethyl radical + HCO, which however is negligible on the triplet PES. The loss of atomic hydrogen can proceed through two distinct transition states (only the minimum energy one, TS2, shown in the PES diagrams), each one with an optical isomer, that differ for the relative position of the O and methyl group in the transition state (cis or trans). The barrier heights are similar (14.8 and 15.1 kcal/mol for the cis and the trans TS), and they thus contribute equally to the reaction kinetics. It is a fast process and the main source of H atoms in the simulated conditions. Decomposition of CH_3CHCH_2O to $^3CH_3CH$ and CH_2O is an important reaction route for the triplet PES since, though the computed energy barrier is higher than that determined for the H loss channels (19.6 vs 14.8 kcal/mol), it has a high pre-exponential factor determined by the presence of two transitional modes with low vibrational frequencies (54.6 and 77.4 cm^{-1}) that were treated as hindered rotors.

Since the present analysis shows that the reactivity that follows addition of oxygen to the terminal C atom is controlled by the kinetics of the entrance well, an extensive search was performed in order to determine whether alternative reaction channels departing from W1 might exist. The reaction routes that were investigated are H_2 formation channels, isomerization to the $^3CH_3CHOCH_2$ ether, and the transfer of oxygen to the central carbon. It was found that the only H_2 formation channels that may compete with the reaction routes already examined are not accessible from W1, though they may be reached through a roaming pathway following H dissociation. The formation of the ether requires overcoming a significant activation energy and was therefore not considered as a viable

reaction route, while no transition state directly connecting W1 and the well that can be accessed from an addition to the central carbon atom (W3) could be found. The reaction route connecting W1 and W3 involves therefore passing from the precursor complex to which both wells are connected.

The reactivity that follows O addition to the central C atom, which leads to the formation of W3 ($^3CH_3CH(O)CH_2$) (see Figure 8), is governed by the competition between decomposition to the methyl + vinoxy radicals via TS9, the loss of the hydrogen atom bound to the central C via TS10, and intersystem crossing (ISC2). The loss of CH_2 from W3 as well as H transfer to oxygen are not competitive with the other three processes because of the high energy barriers. The energy barriers for the loss of CH_3 and H were computed at the CCSD(T)/CBS level as in the first case the T1 diagnostic is small (0.014) and in the second the reaction is quite similar to H loss from W1, where no significant difference between CASPT2 and CCSD(T) energies was found. The energy barrier calculated for decomposition to methyl and vinoxy radicals is 10.4 kcal/mol (TS9), thus significantly smaller than that of H loss (15.2 kcal/mol, TS10), which makes the first process the dominant reaction route for this portion of the PES.

Crossing points between the triplet and the singlet PES were searched on the triplet PES using the same (6e,5o) active space used to study the addition of O to propene and the aug-cc-pVTZ basis set. Spin−orbit couplings (SOCs) have been calculated using orbitals generated through two-state state-averaged CASSCF calculations, using the same active space and basis set used to optimize the structures, and the Breit Pauli operator, as implemented in Molpro.[46] The three coupling elements so determined are then averaged as suggested by Hu et al.[15] SOCs were determined for different geometries and were found to reach a maximum value at the minimum energy crossing point (MECP). The SOCs calculated for ISC from W1 and W3 are 37.4 and 32.1 cm^{-1}, respectively. ISC rates were computed as a function of energy E and momentum J and then averaged over J to give an energy-dependent rate constant $k(E)$ that was used in the simulations. The adopted procedure consists essentially in correcting microcanonical RRKM rate constants with the energy-dependent ISC hopping probabilities calculated with the Landau−Zener model. To perform this calculation, the density of states (DOS) and the activation energy must be computed at the transition state, which in this case was assumed to coincide with the MECP. The DOS depends significantly from the value of the low vibrational frequencies computed at the saddle point. An inspection of the low vibrational modes calculated for the MECP shows that the $CH_3CH−CH_2O$ (ISC1) and $CH_3CHO−CH_2$ (ISC2) torsional vibrations have imaginary frequencies, which were therefore not considered in the calculations, and that two vibrational frequencies of 190 and 614 cm^{-1} correspond to the bending of the C−O bond along the O−C1−C2 plane for ISC from W1 and W3, respectively (see Figure 9 for atom numbering). As it was found that the SOC value decreases significantly even for slight changes of the O−C1−C2 angle, it was decided to not include the 190 and 614 cm^{-1} frequencies in the calculation of the DOS, as their vibrational excitation would most likely lead to significant displacements of the O−C1−C2 angle and thus to the decrease of the ISC probability.

4.2. Reactivity on the Singlet PES after Triplet → Singlet Intersystem Crossing. The structures of the MECP for ISC from W1 and W3 and the PES for ISC from W1 are reported in Figure 9. Following ISC, several reaction routes can
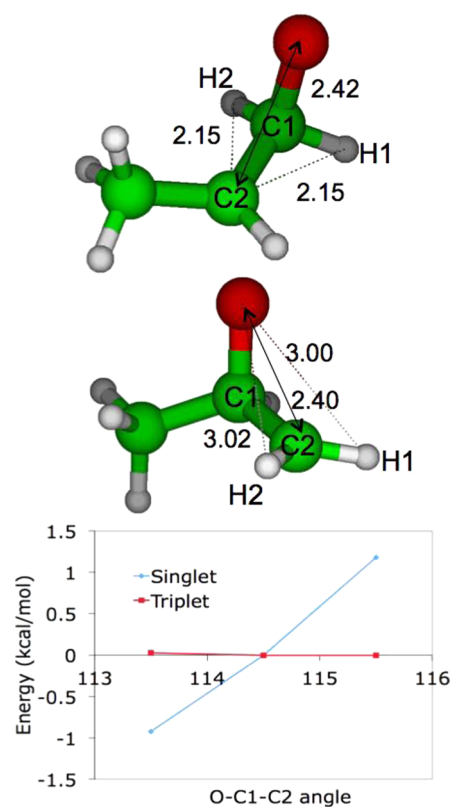
Figure 9. Structures of the MECP for ISC from W1 and W3 and PES for ISC from W1 computed keeping fixed the MECP dihedral angle as a function the O−C1−C2 angle relaxing all the other degrees of freedom.

competitively be accessed from the MECP. The options are two and differ for ISC from W1 and W3. After ISC from W1 two products are possible: methyloxirane and an intermediate unstable state that is connected to several reaction routes (Int1). Methyloxirane may be accessed from the MECP through the formation of the bond between O and C1, which takes place contextually to the decrease of the O−C1−C2 angle. The PES reported in Figure 9 shows indeed that the energy gradient along this internal motion is significant at the MECP. However, the oxygen motion along the O−C1−C2 angle is in competition with the torsional rotation of the CH_2O group around the $CH_3CH−CH_2O$ bond that leads, as shown by an intrinsic reaction coordinate (IRC) analysis, to Int1. The discussion reported at the end of section 4.1 suggests that ISC will take place contextually to the torsional rotation of the CH_2O group, so that the average energy of this internal motion will be probably higher than that for bending along the O−C1−C2 angle, which will be limited for the motivations given above. On the basis of these considerations it was decided to perform the simulations assuming that after intersystem crossing to the singlet surface from W1 both the methyloxirane well and Int1 may be accessed with equal probabilities. A sensitivity analysis, whose results are discussed in section 5.3, has been performed to determine how this assumption impacts the calculation results. The formation of Int1 is consistent with what was found by Nguyen et al.[20] for ethylene, who noticed that after ISC several reaction routes are directly accessible from a metastable singlet intermediate having a structure similar to the MECP though, differently from Nguyen et al., in the present calculations Int1 is not an energy well as it can be

directly converted to propanal without overcoming any energy barrier. It is thus difficult to define unambiguously which is its structure. However, the IRC analysis of the trajectories starting from the saddle points that have been here associated with Int1 shows that they all converge to the same structure, which is similar to that of the MECP of ISC1 with the CH_2O group rotated so that the O atom is in plane with the carbon chain. The reaction routes that can be accessed from Int1, summarized in Figure 10, are conversion to methyloxirane,
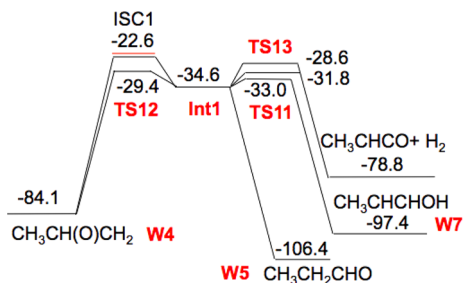
Figure 10. Reaction channels that can be accessed after intersystem crossing from W1. Both *cis* and *trans* channels leading to molecular hydrogen and methylketene are shown as they have similar energies (−31.8 and −28.6 kcal/mol, respectively) and rates, while the two TSs leading to W4 and W5 have almost degenerate energies, and only the most favored (by 2.6 kcal/mol) of the two TSs leading to W7 is shown.

decomposition to molecular hydrogen and methylketene, conversion to 1-propenol, and conversion to propanal. The latter reaction has no distinct transition state, though it has a variational transition state that can be found performing relaxed scans of the PES as a function of the O−C−C angle starting from propanal. Two distinct transition states exist for each reaction channel, each one with two optical isomers, depending on the relative orientation of the O atom and the methyl group (*cis* and *trans*). The *cis* transition states have in general the smallest energy, except for the reactions leading to propanal and methyloxirane, which have nearly degenerate activation energies. The transition state structures that were located for the four possible reaction channels are compared to the MECP structure in Figure 11, where the reported energy of Int1 is assumed to be the same as that of the variational transition state leading to W5. In the present model it is thus assumed that methyloxirane can be accessed from two reaction routes: directly from the MECP structure without passing from Int1 and from Int1. TS structures were determined at the CASPT2 level using a (4e,4o) active space that includes the σ and σ^* orbitals of the two C−O bonds and the aug-cc-pVTZ basis set. Barrier heights for all these reaction channels were determined at the CASPT2 level with reference to the methyloxirane well using a (10e,10o) active space that includes the σ and σ^* orbitals of the two C−O bonds, of the two C−H bonds of the CH_2O group, and of the C1−C2 bond using the aug-cc-pVTZ basis set. Details of CASPT2 calculations are reported in Tables S10−S14 (SI).

The fact that it is difficult to define the Int1 structure poses a problem in the evaluation of the rate of its reaction channels through RRKM theory, which requires the evaluation of the rovibrational density of states of the starting well. However, this is not necessary if the overall reaction flux is known, as this is the case as it is given by the ISC crossing rate, and only branching ratios are necessary. Channel-specific branching
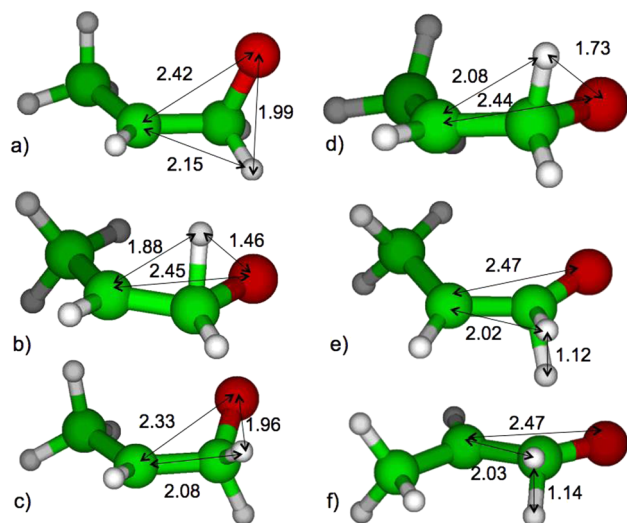

Figure 11. Structures of the transition states of the reaction channels that can be accessed after intersystem crossing from W1: (a) MECP; (b) isomerization to 1-propenol; (c) isomerization to methyloxirane; (d) 300 K canonical variational transition state for isomerization to propanal; (e) and (f) *cis* and *trans* transition states for decomposition to molecular hydrogen and methylketene.

ratios can in fact be computed by weighting the TS density of states $\left(\rho(E^*)_i^{\neq}\right)$ over the sum of the rate of all the possible reaction channels (NC) as

$$BR_i = \frac{\int_0^{E-EA_i} \rho(E^*)_i^{\neq}\,dE^*}{\sum_{i=1}^{NC} \int_0^{E-EA_i} \rho(E^*)_i^{\neq}\,dE^*} \quad (12)$$

Equation 12 can be obtained dividing the RRKM rate constants by the total reaction flux, which is equal to the sum of the rates of all the reaction channels calculated with reference to the same well. The branching ratios among the possible reaction channels that can be accessed from Int1 were calculated as a function of the energy and used in the master equation simulations to partition the ISC flux. The branching ratios so determined are reported in Figure 12 and show that the main reaction channel after ISC, if the system does not react directly to give methyloxirane, is the formation of propanal, followed by
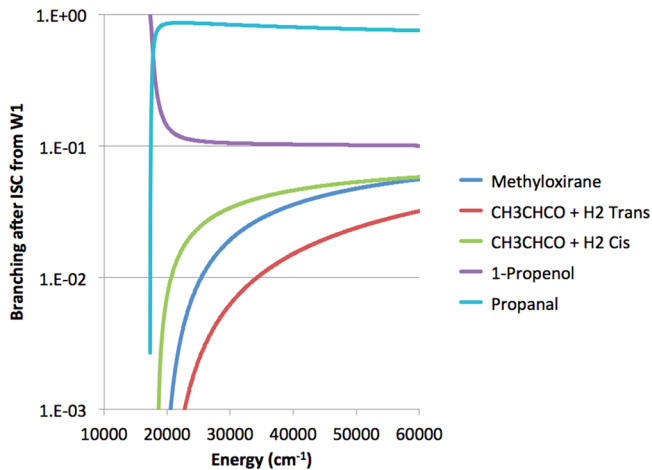
Figure 12. Branching over the reaction channels that can be accessed after ISC from W1 passing through Int1.

1-propenol, while the reaction channel leading from Int1 to methyloxirane is the slowest among the possible reaction routes. Though the decomposition to H_2 and methylketene has a lower weight with respect to the other reaction routes, it is the fastest pathway to methylketene that was found in the present study. The high branching factor for the reaction leading to 1-propenol at low energies is determined by tunnelling effects. The fact that methyloxirane is a relatively slow reaction channel for the reaction flux passing from Int1 supports the assumption made above that methyloxirane may be directly formed after ISC. In fact, experimental results show that methyloxirane and propanal are the collisionally stabilized species that are observed in the highest concentration among the products of the addition of oxygen to propene,[61] thus suggesting that a reaction route faster than that passing from Int1 and leading to methyloxirane should exist.

The reactivity that follows ISC from W3 is much simpler. In this case, no TS leading to propenol or to decomposition products could be found. Similarly to what is done for ISC1, it was thus assumed that ISC from W3 leads to both methyloxirane and acetone with equal probabilities.

4.3. Reactivity on the Singlet PES: Methyloxirane. Methyloxirane (W4) plays a central role in the reactivity on the singlet PES, as it can be accessed from the triplet surface through ISC from both W1 and W3, and as shown in Figure S2 (SI), it is directly connected through TS12 to propanal (W5, and the other reaction channels that can be accessed from Int1:1−propenol and methylketene + H_2), through TS20 to acetone (W6), and through TS18 to an ether (CH_3CHOCH_2, W8, not shown in Figure 8) that can isomerize to vinyl-methyl ether. In addition, W4 can decompose to give ethylene and formaldehyde via TS17. Most of these reactions have a significant multireference character (see Table S5, SI), thus barrier heights and rate constants were determined at the CASPT2 level (except for the TS18, which has a CCSD(T) T1 diagnostic of 0.018). Geometries were computed using a (4e,4o) active space consisting of the σ and σ^* orbitals of the two C−O bonds, while energies were determined increasing systematically the active space up to (10e,10o), as described in detail in Tables S12, S15, and S16 (SI). The calculated energy barriers for isomerization to propanal (through Int1), acetone, and CH_3CHOCH_2 are 54.8, 55.0, and 54.3 kcal/mol, while the barrier for decomposition to ethylene and formaldehyde is 74.8 kcal/mol (TS17). As it can be observed, with the exception of decomposition to ethylene + H_2CO, all the energy barriers are comparable. The high pressure rate constants of methyloxirane interpolated between 300 and 2000 K are reported in Table S17 (SI), while the microcanonical rate constants are compared in Figure 13. It is interesting to observe that the fastest reaction channel is the ring-opening reaction leading to the CH_3CHOCH_2 ether, which is a highly reactive species, having an energy about 42 kcal/mol higher than that of methyloxirane.

4.4. Reactivity on the Singlet PES: Propanal, Acetone, Vinylmethyl Ether, and 1-Propenol. The wells that can be accessed from methyloxirane have several reaction routes that can lead to a large variety of products. The main reaction routes of propanal are isomerization to 1-propenol via TS14, the barrierless decomposition reactions to $C_2H_5 + CH_2O$ and $CH_3 + CH_2CHO$, and decomposition to $H_2 + CO + C_2H_4$ through TS16 and to $CO + C_2H_6$ through TS15. The reactions leading to the formation of the ethyl and methyl radicals are the dominant processes. In particular, the decomposition of propanal to ethyl and HCO is responsible for all the ethyl
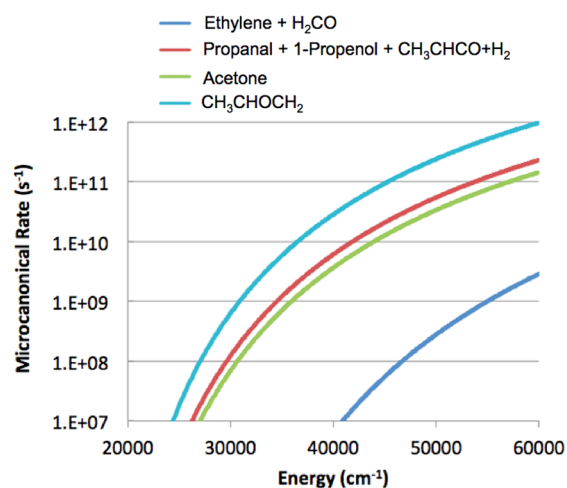
Figure 13. Microcanonical rate constants for the possible reactions of methyloxirane.

radicals in the master equation simulations. As these two reactions are barrierless, their rate constant was determined using microvariational (E,J) resolved transition state theory. In the case of decomposition to methyl and vinoxy radicals two distinct minima were found for the reaction fluxes at different values of the reaction coordinate, which may thus be interpreted as an inner and an outer transition state. The rate constant was in this case determined using two-state transition state theory, which was implemented in the RRKM Master Equation code as suggested by Greenwald et al.[62] The two PESs were computed performing constrained energy minimizations as a function of the breaking bond length. Simulations were performed at the CASPT2(4e,4o)/aug-cc-pVTZ level using as active space the π and π^* orbitals of the C=O bond and the σ and σ^* orbitals of the breaking bond. The calculated energies were scaled to give the reaction energy change calculated at the CCSD(T)/CBS level for the separated products. The PESs of the two reactions are reported in Figure 14.

Both reactions have transitional modes with low vibrational frequencies that were treated in the hindered rotor approx-
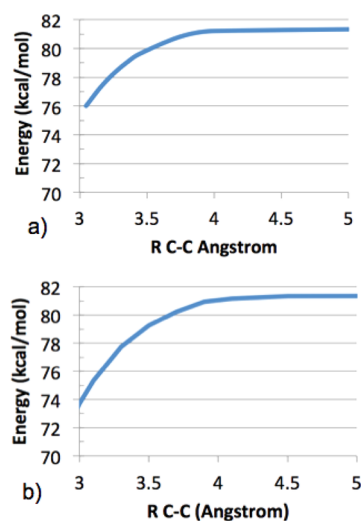
Figure 14. PESs for decomposition of propanal to (a) C_2H_5 + HCO and (b) $CH_3 + CH_2CHO$.

imation. In the decomposition to C_2H_5 and HCO two torsional motions are possible, methyl rotation and ethyl rotation, while for the other reaction channel the only active torsional motion is methyl rotation. In all cases these internal modes were treated in the 1D hindered rotor approximation. A limited sampling of the 2D rotational PES showed that the two internal rotors of the reaction of dissociation to C_2H_5 and HCO are uncoupled.

The decomposition of propanal to ethylene, CO, and H_2 is a three-body process and an important source of hydrogen and ethylene for the thermal simulations performed at 300 K. The reaction of decomposition to CO and ethane is not relevant (BR ≪ 1%) in the investigated conditions.

As has been recently experimentally confirmed,[63] the main reaction route of acetone is decomposition to the methyl and acetyl radicals. Also this reaction is barrierless, and also in this case its rate constant was determined using microcanonical (E,J) resolved transition state theory. The two internal rotors associated with methyl rotation are essentially unhindered both for the reactants and along the reaction coordinate and were therefore treated as unhindered rotors. The reaction PES is reported in Figure S3 (SI). The calculated high-pressure rate constant is in good agreement with the experimental results at 1100 K and 1 bar,[63] which are however overestimated at higher temperatures, probably because of falloff effects.

Two different reaction routes were found for 1-propenol: isomerization to propanal via TS14 and decomposition to methylketene and H_2. TS structures were determined at the CASPT2(6e,6o)/aug-cc-pVTZ level using as active space the σ and σ^* orbitals of the C–O bond and of the two involved C–H bonds. Energies were then computed at the CCSD(T)/CBS level. The fastest reaction channel is isomerization to propanal, as decomposition to methylketene requires overcoming a quite high energy barrier.

The only reaction route of singlet CH_3CHOCH_2 (W8) that is competitive with the rate of the backward reaction leading to methyloxirane is conversion to vinyl-methyl-ether, which takes place through H transfer from methyl to the CH_2 group (see Figure S2, SI). This reaction has an energy barrier of 13.2 kcal/mol, calculated at the CCSD(T)/CBS level, which is only slightly higher than that of conversion to methyloxirane (12.1 kcal/mol). However, the two processes have a considerably different pre-exponential factor that favors the backward reaction. For this reason this reaction route was not included in the master equation simulations.

5. DISCUSSION

We will discuss the experimental results in light of the calculated PESs and of the statistical branching ratios predicted on the coupled triplet and singlet PESs.

5.1. Product Angular Distributions and Lifetimes of Intermediates. It is interesting to note that while for the singlet intermediates RRKM/ME calculated lifetimes are in the range of nanoseconds for the triplet intermediates they are of the order of 10 ps (see Section 5.3) that is much shorter and corresponding to only a few rotational periods of the decomposing complex. Again, within the osculating complex model[57,58] one would expect an asymmetric product angular distribution from triplet channels, as is indeed observed for the two H-elimination channels. Furthermore, it should be noted that the H-elimination channels may not be fully statistical (see below); indeed, only for the BRs of these channels there occur

a quite significant deviation between the experimental values and the statistical predictions (see Table 1).

5.2. Product Recoil Energies and PES. We will refer to the PES shown in Figure 8 which highlights the main reaction pathways for the reaction of $O(^3P)$ with propene. The analysis of the PES is useful in interpreting the experimental evidence, such as the large fractions of energy released in translation that are observed experimentally for some of the channels and that reflect significant exit potential barriers. In fact, following the initial electrophilic attack of the $O(^3P)$ atom to the unsaturated bond of propene on the terminal carbon atom (C1) with an entrance barrier of 0.16 kcal/mol, the initial triplet diradical intermediate CH_3CHCH_2O in part undergoes C–H bond cleavage via TS2 to $CH_3CHCHO + H$ with an exit barrier of about 8.5 kcal/mol (with respect to the product asymptote). Indeed the $P(E'_T)$ of this channel just peaks at this value (see Figure 6, top rhs panel). The average fraction of energy in translation $\langle f_T \rangle$ for the H channels has a value (about 0.38 and 0.23 for the two isomeric channels) quite typical for reactions of this kind with an exit barrier and is in line with previous determinations on related systems, such as for instance those obtained for the corresponding channels in the $O(^3P)$ + propyne reaction where a fraction of 0.38 was derived.[14]

The triplet intermediate CH_3CHCH_2O can also undergo competitively C–C bond rupture with formation of $^3CH_3CH$ + H_2CO via TS3 located only 1.1 kcal/mol with respect to the product asymptote. Because of the small exit barrier we would expect a small fraction of energy in translation: indeed the $P(E'_T)$ for the $H_2CO + {}^3CH_3CH$ channel peaks at only 2.5 kcal/mol but extends somewhat beyond the limits of energy conservation for the triplet channel. This indicates that part of the H_2CO product is actually formed from the singlet PES after ISC, but the relative fractions cannot be disentangled in these measurements. While $\langle f_T \rangle$ would be 0.56 for the $^3CH_3CH$ + H_2CO channel from the triplet PES, it would result in about 0.10 for $C_2H_4 + H_2CO$ from the singlet PES. We will attempt to rationalize the mechanism and BR of the formaldehyde forming channel with the assistance of the statistical calculations (see next section).

The C–C bond-breaking channel leading to HCO + C_2H_5 on the singlet PES (after ISC has occurred) is barrierless and characterized by a very small $\langle f_T \rangle$ (only 0.04) (see Figure 6). This clearly indicates that when two radical fragments are produced the fraction of energy channelled into their internal degrees of freedom is very large. It has been argued in the photodissociation of propanal at 248 nm[64] that the ethyl radical with a large amount of vibrational degrees of freedom is allowed to gain a large internal energy, and therefore there is not enough internal energy left in HCO to undergo decomposition. Because the total available energy of propanal is similar in the bimolecular reaction at E_c = 9.3 kcal/mol, we do not expect that HCO fragments significantly to H + CO either under our experimental conditions. It is interesting to note that the equivalent pathway in the related $O(^3P) + C_2H_4$ reaction, leading to CH_3 + HCO on the singlet PES, is also barrierless on the exit channel and exhibits a small fraction (0.14) of total available energy released as translational energy.[8] Notably, for this channel it was found by QCT calculations on full dimensional PESs of the rotational energy and mode-specific vibrational state distributions of CH_3 and HCO that CH_3 and HCO are not rotationally excited but have very hot vibrational excitations, especially for the bending modes of both products; in addition to the bending excitations, also

considerable stretching excitations of HCO were found.[8] A similar situation is expected to hold for the internal energy distribution of the C_2H_5 + HCO products in $O(^3P)$ + propene.

Once the system has undergone ISC to the singlet PES, the internally excited propanal (CH_3CH_2CHO), besides dissociating to C_2H_5 + HCO, can also dissociate to CH_3 + CH_2CHO without barrier. This singlet pathway to CH_3 formation is however not clearly supported by the derived $P(E'_T)$ distribution (see second from top panel, rhs, in Figure 6), which, as already discussed, reflects mainly a high exit barrier as is the case for the triplet pathway. This is consistent with the results of the master equation analysis, which shows that this is a minor reaction route for propanal (CH_3 is indeed predicted to be formed for about 2/3 from the triplet PES and 1/3 from the singlet PES; see Tables S18−S21, SI). Molecular hydrogen and methylketene can be formed through a three-center H_2 elimination directly after ISC form W1 (via Int1). Because of the very high exit barrier of about 50 kcal/mol this molecular channel is expected to exhibit a very large recoil energy distribution; indeed the $P(E'_T)$ corresponds to $\langle f_T \rangle$ of about 0.35 (see Figure 6). However, this is a minor channel. For the same reason the three-body channel is also minor. Noteworthy, propanal can undergo a three-body dissociation via TS16 to C_2H_4 + H_2 + CO. This process, however, although predicted by RRKM calculations to be very important in the photodissociation at 193 and 157 nm,[65] to date has not been observed in the UV photodissociation of propanal (while it has been observed in the photodissociation of propenal[64,66]).

The product we observe at m/z = 28 is expected to come mainly from the parent of C_2H_4 formed in the H_2CO + $^3CH_3CH$ channel ($^3CH_3CH$ isomerizes very quickly to triplet C_2H_4 because the competitive dissociative channel leading to H + CH_2CH (vinyl) is endoergic by 34 kcal/mol[67] and possibly in the H_2CO + C_2H_4 channel, while negligibly from CO and C_2H_4 from the three-body process.

5.3. Branching Ratios and RRKM/Master Equation Simulations. The experimentally derived branching ratios are reported in Table 1, where they are compared with the results of the RRKM/Master Equation simulations, which were performed using the complete triplet and singlet PESs that are reported in Figures S1 and S2 (SI). The channel-specific branching ratios calculated through the RRKM/Master Equation simulations are reported in Tables S18−S21 (SI). The average lifetimes calculated for the intermediates for addition to the terminal C are 1.30×10^{-11}, 8.99×10^{-12}, 4.67×10^{-9}, 2.65×10^{-9}, 2.55×10^{-10}, and 1.42×10^{-9} s for the H + CH_3CHCHO, $^3CH_3CH$ + H_2CO, CH_3 + CH_2CHO/$COCH_3$, C_2H_5 + HCO, H_2 + CH_3CHCO, and H_2 + C_2H_4 + CO channels, respectively.

Experiments and simulations are in good agreement for what concerns the formation of CH_3 and C_2H_5 and in agreement within the uncertainty limits for $^3CH_3CH/C_2H_4$ and H_2 channels. The total amount of atomic hydrogen is overestimated by the simulations by a factor of 2, and the branching ratio between the two H channels is significantly mispredicted. Despite this discrepancy, the agreement between simulations and experiments is sufficient to let us draw some conclusions on the system reactivity. According to the simulations, ISC to the singlet surface is about 20% at E_c = 9.3 kcal/mol, which is significantly smaller than what was found for ethylene,[7,8] where it was found to be about 50% at comparable collision energies. The theoretical estimation is supported by the prediction that the most abundant products observed in this experiment,

$^3CH_3CH/C_2H_4$ + H_2CO (44% measured and 33% calculated), come from TS3 on the triplet surface which, as reported above, is partially consistent with the recoil energy measured for this channel. In addition, atomic H is produced mostly through TS2 on the triplet PES, and more than 50% of methyl is produced from TS9 following the addition of O to the central carbon atom. Indeed three different channels contribute to the production of methyl, one located on the triplet PES (TS9) and the two barrierless decomposition pathways of propanal and acetone on the singlet. According to the simulations, the C_2H_5 + HCO products are formed entirely on the singlet PES from the decomposition of propanal, while H_2 is produced on the singlet PES both from the decomposition of Int1 to methylketene and from the three-body decomposition of propanal to H_2, C_2H_4, and CO. Quite interestingly, the main reaction channels are C−C bond breaking channels, and that means that the three-carbon chain of propene is not maintained when attacked by atomic oxygen (by an extent larger than 80%; see Table 1). The disagreement between the calculated and measured H branching ratio is well outside the experimental uncertainty and may be due to a H loss channel leading to CH_3COCH_2 that is missing in the PES or to a considerable error in the estimation of the activation energies for the most important channels on the triplet PES. The latter two hypotheses were carefully considered, and no alternative reaction channel or significant error in the calculation of the activation energies on the triplet PES could be found. An interesting alternative hypothesis that may explain the observed difference between calculations and experiments is that at the relatively high translational energies considered in this study (9.3 kcal/mol) the distribution of internal energy that follows the addition of oxygen to propene is nonstatistical, so that dynamic effects rule the H atom formation. Indeed, the two H loss channels are the result of the cleavage of C−H bonds located on the site of addition of the oxygen atom. This behavior is known as non-RRKM, which means that RRKM theory cannot be applied to determine the rate of these processes. An analysis of this hypothesis would require a dynamic simulation as recently done for the simpler $O(^3P)$ + C_2H_4 reaction[7,8] and is therefore outside of the aim of this study.

The comparison of the simulation results performed at 300 K with the experimental data of Koda et al.[29] and Savee et al.[21] is consistent for what concerns the identification of the major reaction channels, which are the production of methyl and ethyl radicals and the formation of molecular hydrogen + methylketene. The methyl branching ratio measured by Koda et al. refers only to the channel having as a parent the vinoxy radical, while the present simulations predict that also the CH_3CO radical can be an important reaction product, accounting for about 40% of the total methyl production. In our CMB experiments it is very difficult to distinguish whether CH_3 is formed from propanal dissociation (with CH_2CHO as coproduct) or from acetone dissociation (with CH_3CO as coproduct). Considering the higher probability of C1 attack with respect to C2 attack we expect that most of the CH_3 from the singlet PES comes from propanal. Taking this into account, the experimental[29] and calculated branching ratios of the CH_3 + CH_2CHO channel are in good agreement (0.29 ± 0.15 vs 0.25), while the relative rate of the C_2H_5 channel with respect to that of the CH_3 channel is slightly underestimated by the simulations (1.39 ± 0.18 vs 1.14). The calculated ethyl production rate is also slightly underestimated with respect to

the CMB experiments and to the kinetics data of Savee et al.,[21] though it is within the uncertainty limits of both experiments. The atomic hydrogen branching ratio predicted by the statistical calculations differs significantly (by a factor of 3) from the data reported by Knyazev et al.,[30] which were used by Savee et al. to determine absolute branching ratios. However, as mentioned in the Introduction, it is known that the H branching ratio determined in the same study for the reference reaction of $O(^3P) + C_2H_4$ is largely overestimated with respect to the established value, which suggests that the present discrepancy may be due to a systematic experimental error. Also, this is consistent with what was found by Washida et al.,[31] who identified $CH_3 + CH_2CHO$ as a major route and $H + CH_3CHCHO$ as a minor route for this system, while according to the branching ratios calculated by Savee et al. on the basis of Knyazev H branching ratio, it should be the opposite. On this basis, it is reasonable to perform the comparison with the data of Savee et al. in terms of branching with respect to the methyl channel (data reported between parentheses in Table 1). Also in this case the $C_2H_5 + CHO$ is slightly underestimated by the simulations, while the $H_2 + CH_3CHCO$ production rate is in good agreement with the experiments and confirms, as proposed by Savee et al. on the basis of deuterated experiments, that the observed H_2 comes from the terminal carbon hydrogen atoms through TS13. In addition, there is agreement with the branching ratio to ethylene (+ H_2CO) predicted by Savee et al.[21] and the one determined in the present simulations. This is interesting as Savee et al. considered the C_2H_4 product as secondary since a mechanistic route that could reconcile the evidence from deuterated experiments could not be found. In the present simulation it is predicted that C_2H_4 is formed as $^3CH_3CH$ through TS3 and as C_2H_4 (via a three-body process) through TS16 in a 2:1 ratio, thus confirming that the reaction kinetics is indeed complex. However, Savee et al. were unable to find the $^3CH_3CH$ signal (mass 28) when experiments were performed using CH_3CHCD_2, which is not consistent with the present mechanism. A possible explanation is that $^3CH_3CH$ may have a significant secondary reactivity with NO_2 (the $O(^3P)$ source) in the kinetics study, which may prevent its isomerization to the more stable ethylene isomer. This would thus explain why in the same experiments the parent D_2CO signal could be observed (it should be noted that for technical reasons the H_2CO species was hard to detect in the kinetics experiment because the precursor of the $O(^3P)$ atoms is NO_2 which gives a strong signal at $m/z = 30$, which corresponds also to the mass of H_2CO).

Some additional calculations were performed to test the effect that a modification of the assumption that after ISC the reaction flux is equally split in two to give Int1 and W4 (or W6) has on the simulation results. For this purpose two simulations were performed for the thermal 300 K system, which is most sensible to the singlet reactivity, assuming that after ISC the reaction flux leads only to Int1 or only to W4 (or W6 for ISC from W3). In the first case the simulations predict a decrease of the CH_3 BR from 0.442 to 0.416 and an increase of the C_2H_5 BR from 0.283 to 0.307, thus slightly improving the agreement with the experiments. In the second sets of simulations the CH_3 BR increases from 0.442 to 0.470, and the C_2H_5 BR decreases from 0.283 to 0.259. The H_2 BR changes proportionally to C_2H_5. On the whole, these results show that the assumption made on the reaction flux splitting after ISC has a small but non-negligible effect on the simulations results.

Finally, it is interesting to examine the trend of the BRs with E_c from room temperature to about 9 kcal/mol, from both experiments and statistical calculations. We will mainly compare the CMB results at E_c = 9.3 kcal/mol with the kinetics results at 300 K (corresponding to about 1 kcal/mol average translational energy). As Table 1 shows, while the BRs of the H_2 and CH_3 channels are, within the error bars, nearly the same at the two translational energies, the experimental BR of the C_2H_5 channel decreases by nearly a factor of 3 by increasing E_c from 1 to 9 kcal/mol. Notably, these trends are fully corroborated by the RRKM calculations which also predict with increasing E_c a little variation of the H and CH_3 channel BRs and a strongly decreasing BR (by nearly a factor 4) for the C_2H_5 channel. We remind that the H channel and about 2/3 of the CH_3 channels are occurring on the triplet PES, while the C_2H_5 channel occurs entirely on the singlet PES. Regarding the H_2CO channel, its BR is found to be large at E_c = 9.3 kcal/mol, in agreement, within the uncertainties, with the theoretical prediction. The experimental BR of 0.44 corresponds to a ratio H_2CO/CH_3 of nearly 1.4; in contrast, at 300 K the yield of H_2CO is much smaller, with a H_2CO/CH_3 ratio of 0.27 ± 0.18, and moreover is attributed mainly to secondary reactions,[21] the contribution of this channel as primary product being estimated to be minor. Notably, the RRKM calculations predict the H_2CO channel to be a primary product also at 300 K, with a H_2CO/CH_3 ratio (0.212) close to the experimental observation (0.27 ± 0.18) (see Table 1). While the statistical absolute BR is predicted to be relatively low (0.065) at 300 K, it is predicted much higher (0.321) at E_c = 9.3 kcal/mol. It remains unclear why the H_2CO channel has not been observed as a primary product in the most recent kinetics work (while it was observed, albeit as minor product, in early experiments[27,28] at essentially room temperature); however, its presence as a primary minor channel could not be ruled out.[21] This channel may warrant further experimental investigation.

Regarding the H elimination channels, these were not detected in the kinetics work,[21] so it is difficult to comment on the trend of these channels with E_c. If we compare the overall CMB BR of the H channels of 0.12 with the kinetics BR estimated by Knyazev et al.[30] of 0.46 ± 0.11 and adopted by Savee et al.[21] to derive absolute BRs, we note a strong decrease, by nearly a factor 4, with increasing E_c. This, however, is contradicted by the RRKM calculations, which find a BR which increases with increasing E_c, from 0.159 at 300 K to 0.261 at 9.3 kcal/mol. Clearly, the BR of 0.46 is strongly overestimated in the kinetics work, as already discussed. Although the theoretical estimate is larger (by a factor 2) than the experimental determination at E_c = 9.3 kcal/mol, it is notable that the H channel yield is predicted to increase with E_c.

Finally, it is interesting to note that the RRKM calculations predict the overall yield of all channels coming from the triplet PES to increase with increasing E_c and those coming from the singlet PES to decrease (from 60% to 20%) with increasing E_c. This corresponds to an extent of ISC which decreases (from 60% to 20%) with increasing E_c, as one would expect from a shortening of the triplet diradical intermediate lifetimes with increasing E_c, and a consequent lower probability of ISC. A similar, although less pronounced, trend of ISC with E_c was also found in the $O(^3P) + C_2H_4$ related system.[7,8]

It is quite interesting to note that the theoretically estimated extent (20%) of ISC in the $O(^3P)$ + propene reaction is less than one-half of that (50%) found in the simpler $O(^3P) + $ ethylene reaction[8] at comparable E_c. Although experimentally

the extent of ISC in O(^{3}P) + propene is thought to be larger than the statistically predicted 20% (because part of the H$_2$CO channel is expected to come from the singlet PES, as already discussed), these results indicate that ISC does not necessarily always increase with increasing molecular complexity. Despite the fact that the triplet diradicals CH$_3$CHCH$_2$O/ CH$_3$CHOCH$_2$ have a stability of −23.7 kcal/mol, slightly larger than the value of −21.5 kcal/mol of the triplet diradical C$_2$H$_4$O in O(^{3}P) + C$_2$H$_4$,[7,8] their probability of ISC to the corresponding singlet species is considerably lower, presumably because a very significant fraction of the reactive flux goes from the more abundant CH$_3$CHCH$_2$O triplet intermediate to the ^{3}CH$_3$CH + H$_2$CO products, a reaction channel which does not have the equivalent in the O(^{3}P) + C$_2$H$_4$ reaction. In contrast, ISC in O(^{3}P) + CH$_2$CCH$_2$ (allene)[15] appears to be larger than in O(^{3}P) + ethylene because the corresponding triplet diradical intermediates are much more stable (more than −60 kcal/mol) with respect to the O + ethylene and O + propene cases. Notably, despite that also in this other three-carbon alkene (actually, the simplest diene) there are competitive C−C bond cleavage channels on the triplet PES, as in O + propene, the much longer lifetime of the triplet intermediate makes much higher the probability of ISC. All this suggests caution in extrapolating the extent of ISC along a series because it appears to be all matter of relative rates of competing pathways, which in turn depend on the detailed topology of the PESs.

6. SUMMARY AND CONCLUSIONS

We have reported a combined experimental and theoretical study on the determination of the primary product channels, their branching ratios, and detailed dynamics for the combustion relevant O(^{3}P) + propene reaction. From crossed molecular beams experiments with soft electron-ionization mass-spectrometric detection at E_c = 9.3 kcal/mol and synergic, high-level *ab initio* electronic structure calculations of stationary points of the underlying triplet and singlet C$_3$H$_6$O potential energy surfaces as well as statistical (RRKM/Master Equation) computations of branching ratios with inclusion of non-adiabaticity (i.e., ISC), we have now a complete picture of the O(^{3}P) + propene reaction. The mechanism sees the initial electrophilic attack of the O atom to the double bond of the CH$_3$CHCH$_2$ molecule on both the terminal and central C atom with formation of the triplet diradical adducts CH$_3$CHCH$_2$O and CH$_3$COHCH$_2$ that under single collision conditions may undergo competitively C−H bond cleavage, C−C bond rupture, isomerization, and intersystem crossing processes, giving rise to a rich variety of product channels. We have characterized the dynamics (center-of-mass product angular and translational energy distributions) of the six main open reaction channels, namely, those leading to CH$_3$CHCHO + H, CH$_3$COCH$_2$ + H, CH$_3$CHCO + H$_2$, CH$_3$ + CH$_2$CHO, C$_2$H$_5$ + HCO, and C$_2$H$_4$/^{3}CH$_3$CH + H$_2$CO. The conclusion is that the reactive interaction of atomic oxygen with propene breaks apart the three-carbon atom chain, mostly producing the radical products methyl + vinoxy (32%) and ethyl + formyl (9%) and the molecular products ethylene/ethylidine + formaldehyde (44%). In addition, two isomeric C$_3$H$_5$O species, CH$_3$CHCHO (7%) and CH$_3$COCH$_2$ (5%), are observed following H atom elimination, which reflects the O atom attack to both the terminal and central C atoms of propene. Finally, also some methylketene (3%) is produced following molecular hydrogen elimination.

As some of the observed products can only be formed via ISC from triplet to singlet PESs, from the product branching ratios we have inferred the extent of ISC. Another important conclusion is that ISC is relevant, accounting for about 20% of the product yield at the experimental collision energy; however, this value is significantly lower than that previously observed in the related reactions O(^{3}P) + ethylene (about 50%) and O(^{3}P) + allene (about 90%). The fact that the extent of ISC in a complex system like O(^{3}P) + propene is lower than in a simpler (fewer atoms) system, as O(^{3}P) + C$_2$H$_4$, and much lower than in a system of similar complexity, as O(^{3}P) + allene, is to some extent a surprising result, which however can be qualitatively rationalized, as discussed, in terms of the differences in the topology and energetic of the corresponding underlying PESs.

Comparison of the branching ratios derived from the CMB experiments at E_c = 9.3 kcal/mol with those obtained from the recent kinetics studies at 300 K and with the RRKM/ME statistical predictions under the two different energetic conditions has provided useful information on the variation of BRs with collision energy (temperature). Overall, the yield of product channels from the singlet PES decreases (from 60% to 20%) with increasing relative translational energy (temperature), as expected on the basis of a shorter lifetime of the intermediate complex with increasing E_c and consequent lower probability of ISC. Notably, the decreasing trend of the extent of ISC from 300 K to E_c ∼ 9 kcal/mol in O(^{3}P) + propene appears to be much more pronounced than in O(^{3}P) + ethylene. All this poses the question of how important it is to consider nonadiabatic effects for this and other similar systems involved in combustion chemistry, warning that simple extrapolations cannot be made.

As pointed out in a recent letter,[22] our combined experimental/theoretical study has provided evidence that the hitherto unidentified channel 6, leading to ^{3}CH$_3$CH + H$_2$CO, is an important reaction channel, and its yield strongly increases with temperature. This channel can be considered the equivalent of the H$_2$CO + ^{3}CH$_2$ forming channel observed in the related O(^{3}P) + C$_2$H$_4$ reaction;[7,8] however, in O(^{3}P) + C$_3$H$_6$ it had never been observed experimentally at combustion temperatures, nor considered to be important, although early works[27,28] found that some H$_2$CO is formed also at room temperature. We note that only recent RRKM predictions (without accounting for ISC) on an *ab initio* triplet PES gave a yield for this channel of about 5% at 300 K and about 24% at 1500 K (at pressure of 0.001 Torr).[34] Our study confirms this trend and, because it accounts for also ISC, assesses it more conclusively. The observation that at combustion temperatures the reactions of O(^{3}P) with alkenes leads to a significant formation of formaldehyde, an important pollutant, is an unexpected result that can have significant practical implications. In fact, the ^{3}CH$_3$CH + H$_2$CO channel appears not to have been included in combustion kinetics models so far, and its introduction may affect the model outcomes.

The CMB results are overall in line with the statistical description of the reaction mechanism obtained by the high-level *ab initio* electronic structure calculations of the coupled triplet and singlet PESs. However, some significant differences between experimental and statistical branching ratios are noted, mainly for the H elimination channels which, however, may not be statistical. A more detailed understanding of the reaction dynamics of this system can only be obtained from QCT-surface hopping calculations on full dimensional, coupled

triplet, and singlet *ab initio* PESs, as recently reported[7,8] for the related $O(^3P) + C_2H_4$ reaction.

The present experimental/theoretical results, which have led to a detailed understanding of the complex mechanism of the $O(^3P)$ + propene reaction, including assessment of the role of ISC, together with the results of the recent kinetics experiments at 300 K, are expected to facilitate the improvement of detailed theoretical models of hydrocarbon combustion.

ASSOCIATED CONTENT

Supporting Information

Active spaces used to optimize structures and determine vibrational frequencies. Triplet and singlet Potential Energy Surfaces used in the Master Equation simulations. High pressure rate constants for entrance channels and H abstraction. CCSD(T)/CBS energies and T1 diagnostic. Details of energy estimations performed at the CASPT level. High pressure rate constants for methyloxirane reaction channels. PES for acetone decomposition to CH_3CO and CH_3. Results of ME/RRKM simulations of CMB experiments. Results of ME/RRKM simulations of thermal experiments (300 K, 4.7 Torr in He). Structures and vibrational frequencies of wells and saddle points. This material is available free of charge via the Internet at http://pubs.acs.org.

AUTHOR INFORMATION

Corresponding Authors
*E-mail: piergiorgio.casavecchia@unipg.it. Phone: (+39) 0755855514.
*E-mail: carlo.cavallotti@polimi.it. Phone: (+39) 0223993176.

Present Addresses
†Faculty of Safety Engineering, VŠB − Technical University of Ostrava, Ostrava, Czech Republic.
‡Institut des Sciences Moléculaires, Université de Bordeaux, UMR 5255 CNRS, 33400 Talence, France.
§Dipartimento di Ingegneria Civile ed Ambientale, Università degli Studi di Perugia, 06125 Perugia, Italy.

Notes
The authors declare no competing financial interest.

REFERENCES

(1) Gardiner, W. C., Jr. *Gas-phase combustion chemistry*; Springer-Verlag: New York, 2000.

(2) Miller, J. A.; Pilling, M. J.; Troe, J. Unravelling Combustion Mechanisms through a Quantitative Understanding of Elementary Reactions. *Proc. Comb. Inst.* **2005**, *30*, 43−88.

(3) Baulch, D. L.; Bowman, C. T.; Cobos, C. J.; Cox, R. A.; Just, Th.; Kerr, J. A.; Pilling, M. J.; Stocker, D.; Troe, J.; Tsang, W.; et al. Evaluated Kinetic Data for Combustion Modeling: Supplement II. *J. Phys. Chem. Ref. Data* **2005**, *34*, 757−1397.

(4) Casavecchia, P.; Leonori, F.; Balucani, N.; Petrucci, R.; Capozza, G.; Segoloni, E. Probing the Dynamics of Polyatomic Multichannel Elementary Reactions by Crossed Molecular Beam Experiments with Soft Electron-Ionization Mass Spectrometric Detection. *Phys. Chem. Chem. Phys.* **2009**, *11*, 46−65.

(5) Lee, S.-H.; Chen, W.-K.; Huang, W.-J. Exploring the Dynamics of Reactions of Oxygen Atoms in States ^3P and ^1D with Ethene at Collision Energy 3 kcal/mol. *J. Chem. Phys.* **2009**, *130*, 054301−13.

(6) Leonori, F.; Balucani, N.; Capozza, G.; Segoloni, E.; Volpi, G. G.; Casavecchia, P. Dynamics of the $O(^3P) + C_2H_2$ Reaction from Crossed Molecular Beam Experiments with Soft Electron Ionization Detection. *Phys. Chem. Chem. Phys.* **2014**, *16*, 10008−22.

(7) Fu, B.; Han, Y.-C.; Bowman, J. M.; Angelucci, L.; Balucani, N.; Leonori, F.; Casavecchia, P. Intersystem Crossing and Dynamics in $O(^3P) + C_2H_4$ Multichannel Reaction: Experiment Validates Theory. *Proc. Natl. Acad. Sci. U.S.A.* **2012**, *109*, 9733−38.

(8) Fu, B.; Han, Y.-C.; Bowman, J. M.; Leonori, F.; Balucani, N.; Angelucci, L.; Occhiogrosso, A.; Petrucci, R.; Casavecchia, P. Experimental and Theoretical Studies of the $O(^3P) + C_2H_4$ Reaction Dynamics: Collision Energy Dependence of Branching Ratios and Extent of Intersystem Crossing. *J. Chem. Phys.* **2012**, *137*, 22A532-1−22.

(9) Alagia, M.; Balucani, N.; Cartechini, L.; Casavecchia, P.; van Beek, M.; Volpi, G. G.; Bonnet, L.; Rayez, J. C. Crossed Beam Studies of the $O(^3P,^1D) + CH_3I$ Reactions: Direct Evidence of Intersystem Crossing. *Faraday Discuss.* **1999**, *113*, 133−150.

(10) Gao, X.; Essex-Lopresti, J.; Munro, S.; Hall, M. P.; Smith, D. J.; Grice, R. Role of Intersystem Crossing in the Reactive Scattering of $O(^3P)$ Atoms with CH_2I_2 Molecules. *J. Chem. Soc., Faraday Trans.* **1998**, *94*, 641−645.

(11) Alagia, M.; Balucani, N.; Casavecchia, P.; Lagana', A.; Ochoa de Aspuru, G.; van Kleef, E. H.; Volpi, G. G.; Lendway, G. On the dynamics of the $O(^1D) + CF_3Br$ reaction. *Chem. Phys. Lett.* **1996**, *258*, 323−329.

(12) Balucani, N.; Stranges, D.; Casavecchia, P.; Volpi, G. G. Crossed Beam Studies of the Reactions of Atomic Oxygen in the Ground ^3P and First Electronically Excited ^1D states with Hydrogen Sulfide. *J. Chem. Phys.* **2004**, *120*, 9571−9582.

(13) Leonori, F.; Occhiogrosso, A.; Balucani, N.; Bucci, A.; Petrucci, R.; Casavecchia, P. Crossed Molecular Beam Dynamics Studies of the $O(^3P)$ + Allene Reaction: Primary Products, Branching Ratios and Dominant Role of Intersystem Crossing. *J. Phys. Chem. Lett.* **2012**, *3*, 75−80.

(14) Balucani, N.; Leonori, F.; Nevrly, V.; Falcinelli, S.; Bergeat, A.; Stranges, D.; Casavecchia, P. Reaction Dynamics and Relative Yields of the H- and CH_3-Displacement Channels in the O + CH_3CCH Reaction. *Chem. Phys. Lett.* **2014**, *602*, 58−62.

(15) Hu, W.; Lendvay, G.; Maiti, B.; Schatz, G. C. Trajectory Surface Hopping Study of the $O(^3P)$ + Ethylene Reaction Dynamics. *J. Phys. Chem. A* **2008**, *112*, 2093−2103.

(16) Schmoltner, A. M.; Chu, P. M.; Brudzynski, R. J.; Lee, Y. T. Crossed Molecular Beam Study of the Reaction $O(^3P) + C_2H_4$. *J. Chem. Phys.* **1989**, *91*, 6926−6936.

(17) Schmoltner, A. M.; Huang, S. Y.; Brudzynski, R. J.; Chu, P. M.; Lee, Y. T. Crossed molecular beam study of the reaction $O(^3P)$+allene. *J. Chem. Phys.* **1993**, *99*, 1644−1653.

(18) Rajak, K.; Maiti, B. Trajectory Surface Hopping Study of the $O(^3P) + C_2H_2$ Reaction Dynamics: Effect of Collision Energy on the Extent of Intersystem Crossing. *J. Chem. Phys.* **2014**, *140*, 044314-1−8.

(19) Nguyen, T. L.; Vereecken, L.; Peeters, J. Quantum Chemical and Theoretical Kinetics Study of the $O(^3P) + C_2H_2$ Reaction: A Multistate Process. *J. Phys. Chem. A* **2006**, *110*, 6696−6706.

(20) Nguyen, T. L.; Vereecken, L.; Hou, X. J.; Nguyen, M. T.; Peeters, J. Potential Energy Surfaces, Product Distributions and Thermal Rate Coefficients of the Reaction of O(^{3}P) with C$_2$H$_4$(X^{1}A$_g$): A Comprehensive Theoretical Study. *J. Phys. Chem. A* **2005**, *109*, 7489−7499.

(21) Savee, J. D.; Welz, O.; Taatjes, C. A.; Osborn, D. L. New Mechanistic Insights to the O(^{3}P) + Propene Reaction from Multiplexed Photoionization Mass Spectrometry. *Phys. Chem. Chem. Phys.* **2012**, *14*, 10140−10423.

(22) Cavallotti, C.; Leonori, F.; Balucani, N.; Nevrly, V.; Bergeat, A.; Falcinelli, S.; Vanuzzo, G.; Casavecchia, P. Relevance of the Channel Leading to Formaldehyde + Triplet Ethylidene in the O(^{3}P) + Propene Reaction under Combustion Conditions. *J. Phys. Chem. Lett.* **2014**, *5*, 4213−4218.

(23) Sabbah, H.; Biennier, L.; Sims, I. R.; Georgievskii, Y.; Klippenstein, S. J.; Smith, I. W. M. Understanding Reactivity at Very Low Temperatures: The Reactions of Oxygen Atoms with Alkenes. *Science* **2007**, *317*, 102−105.

(24) Avramenko, L. I.; Kolesnikova, R. V. Mechanisms and Rate Constants of Elementary Gas Phase Reactions Involving Hydroxyl and Oxygen Atoms. In *Advances in Photochemistry*; Interscience: New York, 1964; Vol. 2, p 25.

(25) Cvetanovic, R. J. Addition of Atoms to Olefins in the Gas Phase. In *Advances in Photochemistry*; Interscience: New York, 1963; Vol. 1, pp 115−182.

(26) Cvetanovic, R. J.; Singleton, D. L. Reaction of Oxygen Atoms with Olefins. *Rev. Chem. Intermed.* **1984**, *5*, 183−226.

(27) Kanofsky, J. R.; Gutman, D. Direct Observation of the Products Produced by the O-Atom Reactions with Ethylene and Propylene Studied in High-Intensity Molecular Beams. *Chem. Phys. Lett.* **1972**, *15*, 236−239.

(28) Blumenberg, B.; Hoyerman, K.; Sievert, R. *Primary Products in the Reactions of Oxygen Atoms with Simple and Substituted Hydrocarbons.* Sixteenth Symposium (International) on Combustion; The Combustion Institute: Pittsburgh, 1976, 841−852.

(29) Koda, S.; Endo, Y.; Tsuchiya, S.; Hirota, E. Branching Ratios in O(^{3}P) Reactions of Terminal Olefins Studied by Kinetic Microwave Absorption Spectroscopy. *J. Phys. Chem.* **1991**, *95*, 1241−1244.

(30) Knyazev, V. D.; Arutyunov, V. S.; Vedeneev, V. I. The Mechanism of O(^{3}P) Atom Reaction with Ethylene and other Simple Olefines. *Int. J. Chem. Kinet.* **1992**, *24*, 545−561.

(31) Washida, N.; Inomata, S.; Furubayashi, M. Laser-Induced Fluorescence of Methyl Substituted Vinoxy Radicals and Reactions of Oxygen Atoms with Olefins. *J. Phys. Chem. A* **1998**, *102*, 7924−7930.

(32) Quandt, R.; Min, Z.; Wang, X.; Bersohn, R. Reactions of O(^{3}P) with Alkenes: H, CH$_2$CHO, CO, and OH Channels. *J. Phys. Chem. A* **1998**, *102*, 60−64.

(33) Zhang, W.; Du, B.; Feng, C. An Ab Initio Dynamics Study on the Reaction of O(^{3}P) with CH$_3$CH=CH$_2$ (^{1}A′). *J. Mol. Struct.: THEOCHEM* **2007**, *806*, 121−129.

(34) DeBoer, G. D.; Dodd, J. A. Ab Initio Energies and Product Branching Ratios for the O + C$_3$H$_6$ Reaction. *J. Phys. Chem. A* **2007**, *111*, 12977−12984.

(35) Alagia, M.; Balucani, N.; Casavecchia, P.; Stranges, D.; Volpi, G. G. Reactive Scattering of Atoms and Radicals. *J. Chem. Soc., Faraday Trans.* **1995**, *91*, 575−596.

(36) Balucani, N.; Capozza, G.; Leonori, F.; Segoloni, E.; Casavecchia, P. Crossed Molecular Beam Reactive Scattering: From Simple Triatomic to Multichannel Polyatomic Reactions. *Int. Rev. Phys. Chem.* **2006**, *25*, 109−163.

(37) Alagia, M.; Aquilanti, V.; Ascenzi, D.; Balucani, N.; Cappelletti, D.; Cartechini, L.; Casavecchia, P.; Pirani, F.; Sanchini, G.; Volpi, G. G. Magnetic Analysis of Supersonic Beams of Atomic Oxygen, Nitrogen and Chlorine Generated from a Radio-Frequency Discharge. *Israel J. Chem.* **1997**, *37*, 329−342.

(38) Leonori, F.; Hickson, F.; Le Picard, K. M.; Wang, S. D.; Petrucci, X.; Foggi, R.; Balucani, P.; Casavecchia, N.; Crossed-Beam Universal-Detection, P. Reactive Scattering of Radical Beams Characterized by Laser-Induced-Fluorescence: the Case of C$_2$ and CN. *Mol. Phys.* **2010**, *108*, 1097−1113.

(39) Sibener, S. J.; Buss, R. J.; Ng, C. Y.; Lee, Y. T. Development of a Supersonic O(^{3}P$_J$), O(^{1}D$_2$) Atomic Oxygen Nozzle Beam Source. *Rev. Sci. Instrum.* **1980**, *51*, 167−182.

(40) Lee, Y. T. Reactive Scattering I: Nonoptical Methods. In *Atomic and Molecular Beam Methods*; Scoles, G., Ed.; Oxford University Press: New York, USA, 1987; Vol. 1, pp 553−568.

(41) Casavecchia, P.; Liu, K.; Yang, X. Reactive Scattering: Reactions in Three Dimensions. In *Tutorials in Molecular Reaction Dynamics*; Brouard, M., Vallance, C., Eds.; Royal Society of Chemistry Publishing: Cambridge, UK, 2010; Ch. VI, pp 167−213.

(42) Werner, H. J. Third-order Multireference Perturbation Theory—the CASPT3Method. *Mol. Phys.* **1996**, *89*, 645−661.

(43) Celani, P.; Werner, H. J. Multireference Perturbation Theory for Large Restricted and Selected Active Space Reference Wave Functions. *J. Chem. Phys.* **2000**, *112*, 5546−5557.

(44) Woon, D. E.; Dunning, T. H. Gaussian Basis Sets for Use in Correlated Molecular Calculations. V. Core-Valence Basis Sets for Boron Through Neon. *J. Chem. Phys.* **1995**, *103*, 4572−4585.

(45) Martin, J. M. L. Ab Initio Total Atomization Energies of Small Molecules — Towards the Basis Set Limit. *Chem. Phys. Lett.* **1996**, *259*, 669−678.

(46) Werner, H.-J.; Knowles, P. J.; Lindh, R.; Manby, F. R.; Schütz, M.; Celani, P.; Korona, T.; Mitrushenkov, A.; Rauhut, G.; Adler, T. B.; et al. *MOLPRO* 2008.1.

(47) Barbato, A.; Seghi, C.; Cavallotti, C. An *Ab Initio* Rice-Ramsperger-Kassel-Marcus/Master Equation Investigation of *SiH$_4$* Decomposition Kinetics Using a Kinetic Monte Carlo Approach. *J. Chem. Phys.* **2009**, *130*, 074108-1−11.

(48) Polino, D.; Cavallotti, C. Fulvenallene Decomposition Kinetics. *J. Phys. Chem. A* **2011**, *115*, 10281−10289.

(49) Miller, J. A.; Klippenstein, S. J.; Raffy, C. Solution of Some One- and Two-dimensional Master Equation Models for Thermal Dissociation: The Dissociation of Methane in the Low-Pressure Limit. *J. Phys. Chem. A* **2002**, *106*, 4904−4913.

(50) Fascella, S.; Cavallotti, C.; Rota, R.; Carrà, S. Quantum Chemistry Investigation of Key Reactions Involved in the Formation of Naphthalene and Indene. *J. Phys. Chem. A* **2004**, *108*, 3829−3843.

(51) Eckart, C. The Penetration of a Potential Barrier by Electrons. *Phys. Rev.* **1930**, *35*, 1303−1309.

(52) Cavallotti, C.; Polino, D.; Frassoldati, A.; Ranzi, E. Analysis of Some Reaction Pathways Active During Cyclopentadiene Pyrolysis. *J. Phys. Chem. A* **2012**, *116*, 3313−3324.

(53) Gupte, K. S.; Kiefer, J. H.; Tranter, R. S.; Klippenstein, S. J.; Harding, L. B. Decomposition of Acetaldehyde: Experiment and Detailed Theory. *Proc. Combust. Inst.* **2007**, *31*, 167−174.

(54) Zener, C. Non-Adiabatic Crossing of Energy Levels. *Proc. R. Soc. London Ser. A* **1932**, *137*, 696−702.

(55) Harvey, J. N. Understanding the Kinetics of Spin-Forbidden Chemical Reactions. *Phys. Chem. Chem. Phys.* **2007**, *9*, 331−343.

(56) Polino, D.; Barbato, A.; Cavallotti, C. Toluene and Benzyl Decomposition Mechanisms: Elementary Reactions and Kinetic Simulations. *Phys. Chem. Chem. Phys.* **2010**, *12*, 10622−10632.

(57) Miller, W. B.; Safron, S. A.; Herschbach, D. R. Exchange Reactions of Alkali Atoms with Alkali Halides: a Collision Complex Mechanism. *Discuss. Faraday Soc.* **1967**, *44*, 108−122.

(58) Fisk, G. A.; McDonald, J. D.; Herschbach, D. R. General Discussion. *Discuss.Faraday Soc.* **1967**, *44*, 228−229.

(59) Fitch, W. L.; Sauter, A. D. Calculation of Relative Electron Impact Total Ionization Cross Sections for Organic Molecules. *Anal. Chem.* **1983**, *55*, 832−835.

(60) Tsang, W. J. Chemical Kinetic Data Base for Combustion Chemistry. Part V: Propene. *J. Phys. Chem. Ref. Data* **1991**, *20*, 221−273.

(61) Atkinson, R. Gas Phase Tropospheric Chemistry of Volatile Organic Compounds: 1. Alkanes and Alkenes. *J. Phys. Chem. Ref. Data* **1997**, *26*, 215−290.

(62) Greenwald, E. E.; North, S. W.; Georgievskii, Y.; Klippenstein, S. J. A Two Transition State Model for Radical−Molecule Reactions: A Case Study of the Addition of OH to C_2H_4. *J. Phys. Chem. A* **2005**, *109*, 6031−6044.

(63) Lam, K. Y.; Ren, W.; Pyun, S. H.; Farooq, A.; Davidson, D. F.; Hanson, R. K. Multi-Species Time-History Measurements During High-Temperature Acetone and 2-Butanone Pyrolysis. *Proc. Combust. Inst.* **2013**, *34*, 607−615.

(64) Chaudhuri, C.; Lee, S.-H. A Complete Look at the Multi-Channel Dissociation of Propenal Photoexcited at 193 nm: Branching Ratios and Distributions of Kinetic Energy. *Phys. Chem. Chem. Phys.* **2011**, *13*, 7312−7321.

(65) Chin, C.-H.; Lee, S.-H. Comparison of Two-Body and Three-Body Decomposition of Ethanedial, Propanal, Propenal, n-Butane, 1-Butene, and 1,3-Butadiene. *J. Chem. Phys.* **2012**, *136*, 024308-1−11.

(66) Dey, A.; Fernando, R.; Suits, A. G. State-Resolved Imaging of CO from Propenal Photodissociation: Signatures of Concerted Three-Body Dissociation. *J. Chem. Phys.* **2014**, *140*, 154301-1−7.

(67) Leonori, F.; Skouteris, D.; Petrucci, R.; Casavecchia, P.; Rosi, M.; Balucani, N. Combined Crossed Beam and Theoretical Studies of the $C(^1D) + CH_4$ Reaction. *J. Chem. Phys.* **2013**, *138*, 024311-1−11.